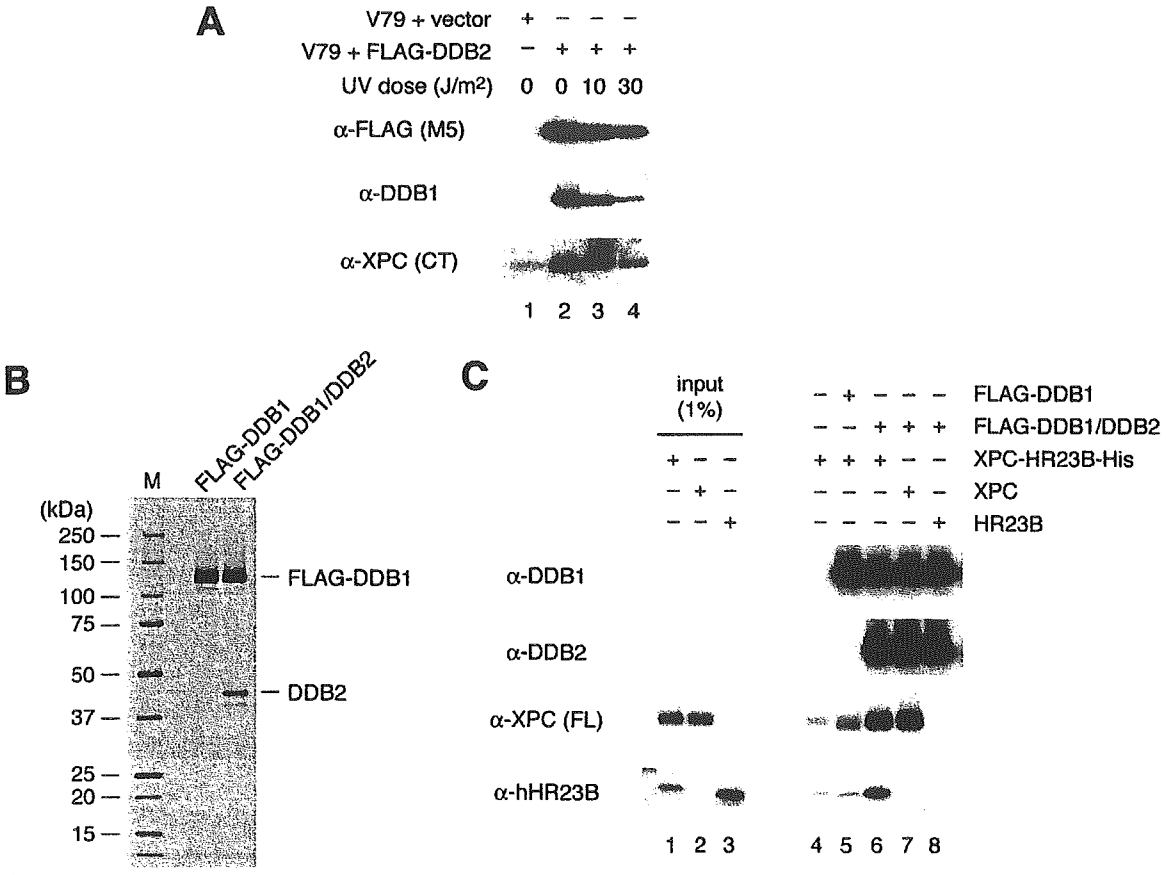

Figure 3. XPC Physically Interacts with UV-DDB

(A) The V79 transformant expressing FLAG-DDB2 was UV irradiated at the indicated dose (lanes 2–4). After incubation at 37°C for 1 hr, soluble cell extracts were prepared, FLAG-DDB2 was immunoprecipitated with anti-FLAG antibody beads, and aliquots of the bound fractions were subjected to immunoblot analyses with the indicated antibodies. As a negative control, the unirradiated, V79 transformant containing the vacant expression vector was processed in the same way (lane 1).

(B) Purification of recombinant UV-DDB. Purified FLAG-DDB1 (150 ng) and FLAG-DDB1/DDB2 heterodimer (200 ng) were subjected to SDS-PAGE (with a 4%–20% gradient gel) followed by silver staining. M, molecular weight markers.

(C) Anti-FLAG antibody beads (20 μl) prebound to either FLAG-DDB1 (1.3 μg) or FLAG-DDB1/DDB2 (1.8 μg) were incubated with XPC-HR23B-His (150 ng), XPC alone (103 ng), or HR23B alone (47 ng). After unbound materials were washed out, aliquots of the bound proteins were subjected to immunoblot analyses using the indicated antibodies (lanes 4–8). One percent of the input XPC and/or HR23B proteins were loaded onto the same gel as controls (lanes 1–3).

UV-DDB Physically Interacts with XPC

The above findings indicating some functional interaction between XPC and UV-DDB prompted us to examine whether they interacted physically as well. When FLAG-DDB2 in the stable V79 transformant was immunoprecipitated from soluble cell extracts, both DDB1 and endogenous XPC were coprecipitated (Figure 3A). This suggests that UV-DDB indeed interacts with XPC in vivo. This interaction was present in both unirradiated and irradiated cells, although UV irradiation significantly reduced the amount of UV-DDB and XPC that was precipitated. This is probably because UV-DDB becomes tightly bound to the UV-induced lesions and thus is not soluble during the extraction procedure (Otrin et al., 1997).

To demonstrate a direct interaction between XPC and UV-DDB, binding experiments were carried out using purified recombinant proteins. FLAG-DDB1 and DDB2 proteins were coexpressed in insect cells using the baculovirus system. With our baculovirus construct, FLAG-DDB1 was expressed in a large excess over DDB2, enabling us to separately purify the FLAG-DDB1/DDB2 complex and free FLAG-DDB1 from the same infected cell extract (Figure 3B). Either the purified UV-DDB complex or FLAG-DDB1 was bound to anti-FLAG antibody beads, which were then incubated with purified XPC-HR23B-His complex. A significant amount of XPC-HR23B-His coprecipitated with the UV-DDB complex, while its binding to FLAG-DDB1 alone was close to background levels (Figure 3C, compare lane 6 with lanes 4 and 5). This indicates that DDB2 is required for the interaction of UV-DDB with XPC. When XPC and HR23B were added separately to the UV-DDB heterodimer, only XPC was detected in the bound frac-

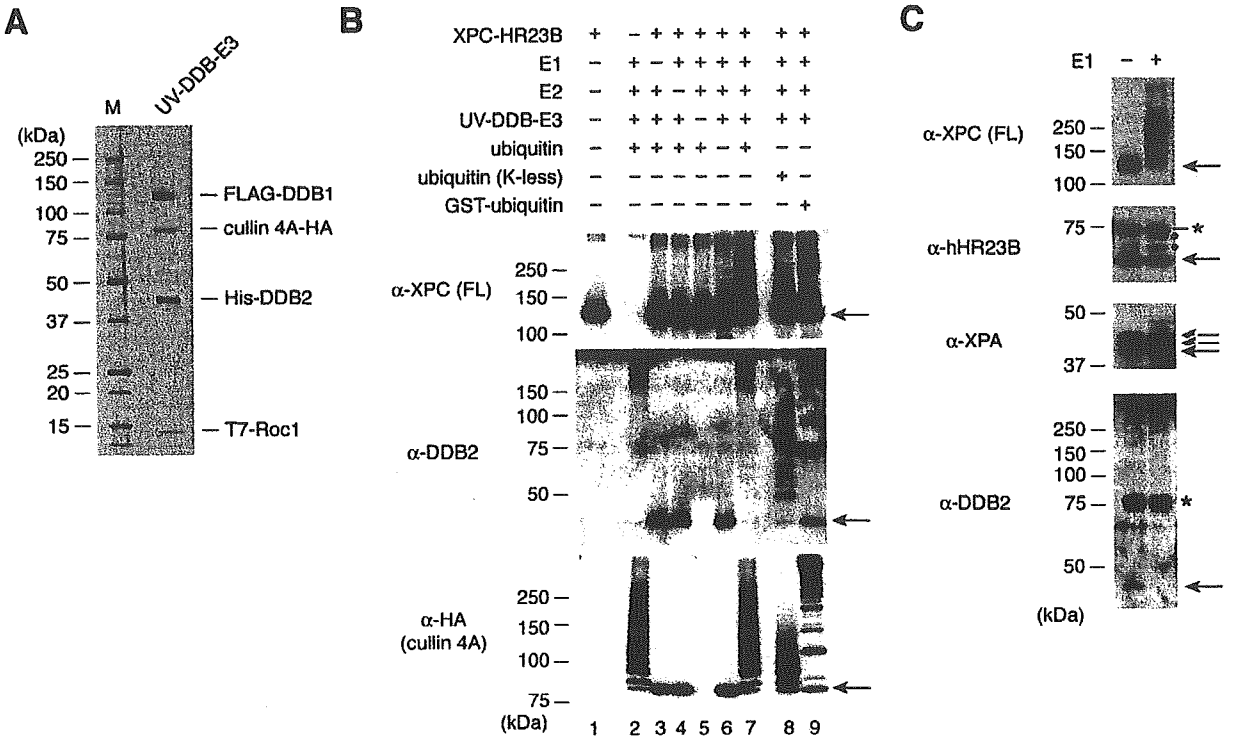

Figure 4. Cell-Free Ubiquitylation of XPC Mediated by the UV-DDB-E3 Complex

(A) The purified UV-DDB-E3 complex was subjected to SDS-PAGE (with a 4%–20% gradient gel) followed by silver staining. M, molecular weight markers.

(B) Cell-free ubiquitylation reactions were performed using the indicated sets of protein components. Where indicated, K-less ubiquitin (5 μg) or GST-ubiquitin (10 μg) was included instead of wild-type ubiquitin (lanes 8 and 9). Aliquots of the reaction mixtures were subjected to immunoblot analyses using the indicated antibodies. The arrows (also those in [C]) indicate the unmodified form of each protein.

(C) A mixture of XPC-HR23B-His (8 ng) and FLAG-XPA (5 ng) was included in the ubiquitylation reaction described in (B) in the absence or presence of E1. Aliquots of the reaction mixtures were subjected to immunoblotting with the indicated antibodies. The asterisk indicates nonspecifically crossreacting bands. The bands indicated by dots represent HR23B-His that had undergone low levels of ubiquitylation.

tion (lanes 7 and 8). These data demonstrate a direct physical interaction between XPC and UV-DDB.

The UV-DDB-E3 Complex Catalyzes the Ubiquitylation of XPC In Vitro

It has been recently reported that UV-DDB exists in vivo as a supercomplex containing cullin 4A and Roc1 that displays ubiquitin ligase (E3) activity (Groisman et al., 2003). This, together with our data, strongly suggests that the UV-DDB-E3 complex may be responsible for the ubiquitylation of XPC. To test this idea, cell-free ubiquitylation assays were carried out. The four subunits (DDB1, DDB2, cullin 4A, and Roc1) were expressed simultaneously in insect cells, and the heterotetrameric complex was purified (Figure 4A). When XPC-HR23B-His was incubated with this UV-DDB-E3 complex in the presence of E1, E2 (UbcH5a), ubiquitin, and ATP, a shift in the molecular weight of XPC was detected (Figure 4B). The shift appeared to depend on each of the protein components (lanes 2–7). The use of GST-tagged ubiquitin instead of normal ubiquitin resulted in an altered pattern of the shifted XPC bands (lane 9), strongly suggesting that the observed band shift is due to conjugation to ubiquitin. Furthermore, when a mutant ubiquitin in which all the lysine residues were changed to arginines (designated "K-less" ubiquitin) was employed in the reaction, the band shift was significantly reduced (lane 8), suggesting that the slow mobility species shown in lane 7 were the result of polyubiquitin chain formation. In the same reactions, DDB2 and cullin 4A were found to be ubiquitylated extensively as well, regardless of the presence or absence of XPC-HR23B-His (Figure 4B, lanes 2 and 7).

To examine the specificity of this in vitro ubiquitylation, XPC-HR23B-His and FLAG-XPA were simultaneously included in the reaction. While XPC and DDB2 were ubiquitylated extensively, little band shifting was observed with FLAG-XPA (Figure 4C) and DDB1 (data not shown) in the same reaction. Although a low percentage of HR23B-His appeared to be conjugated to one or two ubiquitin moieties (see bands indicated by dots in Figure 4C), the band shifting was nonetheless much less pronounced than XPC and DDB2. Thus, the in vitro ubiquitylation system appeared to retain similar substrate specificity as observed in the UV-irradiated cells (Figure 1B).

Since XPC and DDB2 were ubiquitylated in vitro by the same E3 complex, the in vivo fates of the two proteins after UV irradiation were compared. To do this,

we used the V79 transformant expressing FLAG-DDB2, since the available anti-DDB2 antibodies cannot detect endogenous DDB2 expressed in human cells with sufficient sensitivity. When the cells were UV irradiated and incubated in the presence of cycloheximide, XPC underwent reversible modification (lanes 1–6 in Figure S3) exactly as observed in the WI38 VA13 cells. In contrast, the FLAG-DDB2 band decreased in a time-dependent manner and had disappeared almost completely by 4 hr of postirradiation. This decrease in FLAG-DDB2 was blocked when the cells were treated simultaneously with the proteasome inhibitor MG132 (lanes 7–12). Therefore, in agreement with the previous reports (Fitch et al., 2003a; Rapic'-Otrin et al., 2002), DDB2 appeared to be degraded after UV irradiation by the ubiquitin/proteasome system.

Ubiquitylation Alters the DNA Binding Properties of XPC and UV-DDB

To obtain insights into roles the ubiquitylation plays in NER, we examined the DNA binding properties of ubiquitylated XPC and UV-DDB. For this purpose, a synthetic oligonucleotide containing a single UV lesion (CPD or 6-4PP) or the undamaged sequence as a control (Figure S4A) was annealed to the complementary oligonucleotide, tandemly ligated, and immobilized on paramagnetic beads. Cell-free ubiquitylation reactions were carried out in the presence of one of these DNA beads. After unbound fractions were saved and the beads were washed, the proteins retained by the DNA were subjected to immunoblotting for detection of XPC as well as subunits of the UV-DDB-E3 complex (Figure 5A).

When XPC alone was incubated with the DNA beads, only a part of the input protein was detected in the bound fractions (lanes 1–3). We have shown previously (Sugasawa et al., 2001) and in Figure S4B by using the electrophoretic mobility shift assay that XPC specifically binds to 6-4PP and not to CPD, when XPC was added in excess over the damaged DNA; the addition of appropriate competitor DNA was also necessary to absorb the nonspecific DNA binding activity of XPC so that its binding specificity could be unveiled. The binding specificity of XPC for 6-4PP was not as evident in the DNA binding assay shown in Figure 5A, probably because the protein:DNA ratio was much lower and competitor DNA was not included. The presence of the UV-DDB-E3 complex did not affect the binding properties of XPC if ubiquitylation did not occur (Figure 5A, lanes 4–6). In the same reactions, both DDB1 and DDB2 were bound to the 6-4PP beads in a nearly quantitative manner (lane 6), while little binding was observed with the undamaged DNA beads (lane 4). Both the affinity and specificity of UV-DDB for 6-4PP thus seemed to be far higher than those of XPC. The binding of UV-DDB to CPD was also observed, although the affinity appeared to be much lower than that for 6-4PP, as expected from previous reports (Fujiwara et al., 1999; Reardon et al., 1993; Treiber et al., 1992) and our mobility shift assays (Figure S4C). In addition, a significant amount of cullin 4A remained in the unbound fraction even in the presence of the 6-4PP beads (Figure 5A, lane 6), suggesting a somewhat unstable association of the E3 subunit with the UV-DDB core.

Intriguingly, when all factors required for ubiquitylation were present, only ubiquitylated XPC was detected in the DNA bound fractions, although a significant part of XPC still remained unmodified in the unbound fraction (Figure 5A, lanes 7–9). It was also notable that the bands of XPC and cullin 4A were shifted into higher molecular weight regions in the presence of 6-4PP, unlike with undamaged DNA or CPD beads (compare lane 9 with lanes 7 and 8). Thus, although the addition of DNA was not essential for E3 activity (Figure 4), the presence of 6-4PP seemed to stimulate the UV-DDB-dependent ubiquitylation. In these reactions, DDB2 was extensively ubiquitylated, and very little DDB1 or DDB2 was detected in the bound fractions with any of the DNA beads (lanes 7–9). Thus, the ubiquitylation of UV-DDB abolished its DNA binding activity almost completely. In contrast, UV-DDB still retained its DNA binding activity as well as specificity for the UV lesions when methylated ubiquitin was included instead of normal ubiquitin (lanes 10–12), while DDB2 still showed significant band shifts. Reductive methylation of lysine residues in ubiquitin blocks the elongation of polyubiquitin chains (compare the patterns of band shifting in lanes 7–9 with those in lanes 10–12). These data indicate that the formation of polyubiquitin chains above a certain length abrogate the damage binding activity of UV-DDB, whereas polyubiquitylated XPC retains its ability to bind DNA.

To quantitatively examine the effects of ubiquitylation on the DNA binding of XPC, various amounts of XPC-HR23B-His were included in the reaction (Figure 5B). At all doses of XPC tested, ubiquitylation resulted in an about 2-fold increase in the XPC that was retained by DNA beads. However, this effect was observed with undamaged DNA beads as well as with 6-4PP beads (see quantitative data in Figure 5C) and CPD beads (data not shown). Therefore, ubiquitylation appeared to augment the DNA binding of XPC rather than to alter its specificity.

Effects of Ubiquitylation on Cell-Free NER Incision

Finally, we investigated the effects of the ubiquitylation mediated by the UV-DDB-E3 complex on the cell-free NER incision reaction. For this purpose, we prepared a whole-cell extract from the human lymphoblastoid cell line GM01646, which was derived from an XP group E patient. An internally ^{32}P-labeled double-stranded circular DNA substrate containing a single 6-4PP was first preincubated with various amounts of UV-DDB (FLAG-DDB1/DDB2 heterodimer). The mixtures were then incubated with the XP-E cell extract (100 μg of protein), and the labeled dual incision products containing the lesion were separated and detected by denaturing PAGE. As shown in Figure 6A, the preincubation with UV-DDB had little effect on the dual incision around 6-4PP in the cell extract under the conditions tested (lanes 1–4). However, when 20 μg of methylated ubiquitin was added, UV-DDB inhibited the repair of 6-4PP in a dose-dependent manner (lanes 9–12; see also quantitative data in Figure 6B). This inhibition was much less pronounced in the presence of the same amount of normal ubiquitin (lanes 5–8) but similar to when K-less ubiquitin was substituted for methylated ubiquitin (data

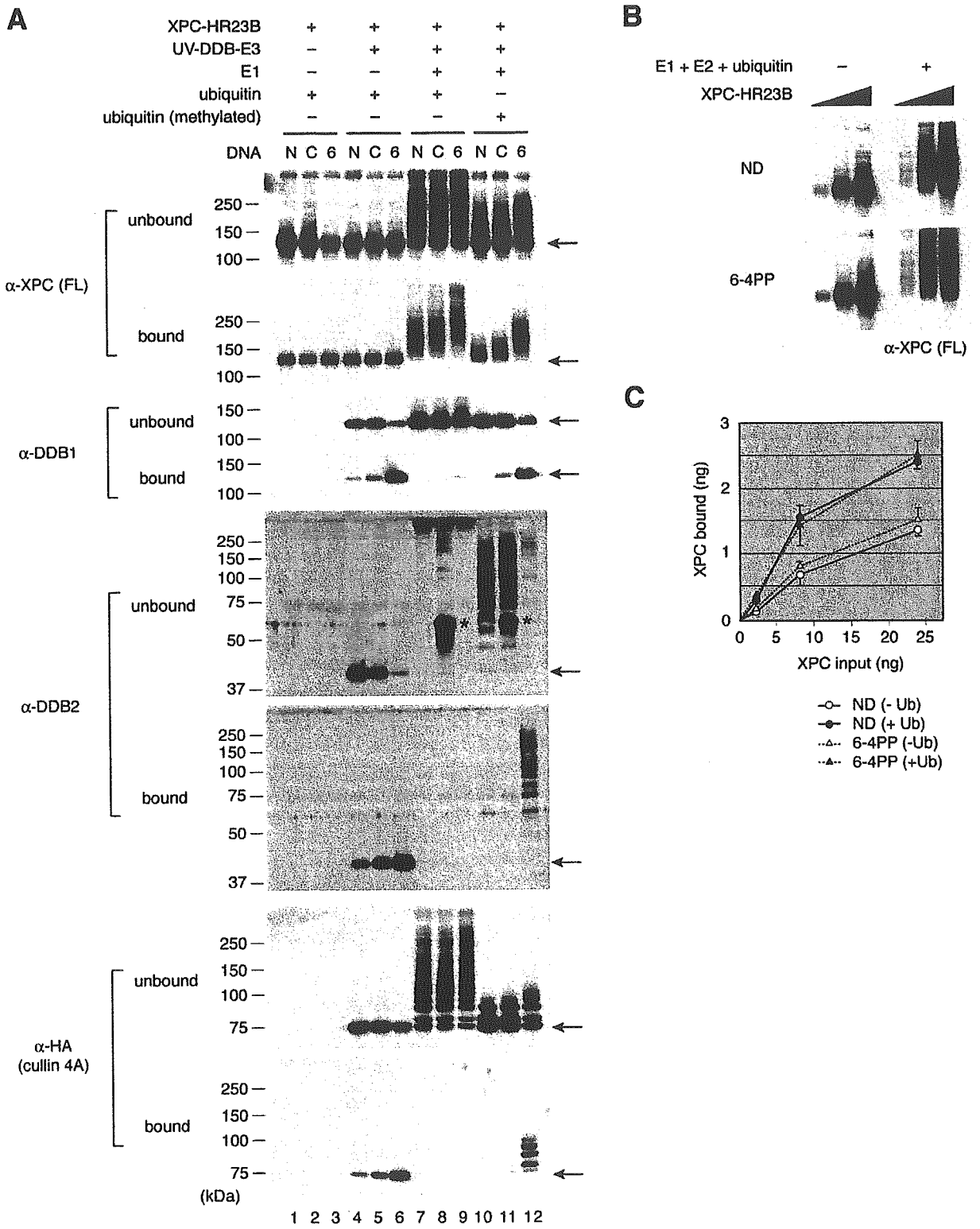

Figure 5. Ubiquitylation Alters the DNA Binding Properties of XPC and UV-DDB

(A) XPC-HR23B-His (8 ng) was incubated with paramagnetic beads bearing undamaged DNA (N) or DNA containing CPD (C) or 6-4PP (6). UV-DDB-E3 (20 ng), and other factors required for ubiquitylation were also included as indicated. The proteins that did not bind to DNA (unbound) and those retained by DNA (bound) were subjected to immunoblot analyses using the indicated antibodies. The arrows indicate the unmodified form of each protein. The asterisks indicate crossreacting bands derived from contaminating keratin.

(B) Binding reactions were performed with undamaged (ND) DNA beads or 6-4PP beads as described in (A) except that the XPC-HR23B-His levels varied (2.4, 8, and 24 ng). The XPC protein that was retained on the DNA beads is shown.

(C) The bound XPC levels in (B) were quantified by comparison with the signals of known amounts of XPC and plotted as a graph. The mean ± standard error of the mean was calculated from two independent experiments.

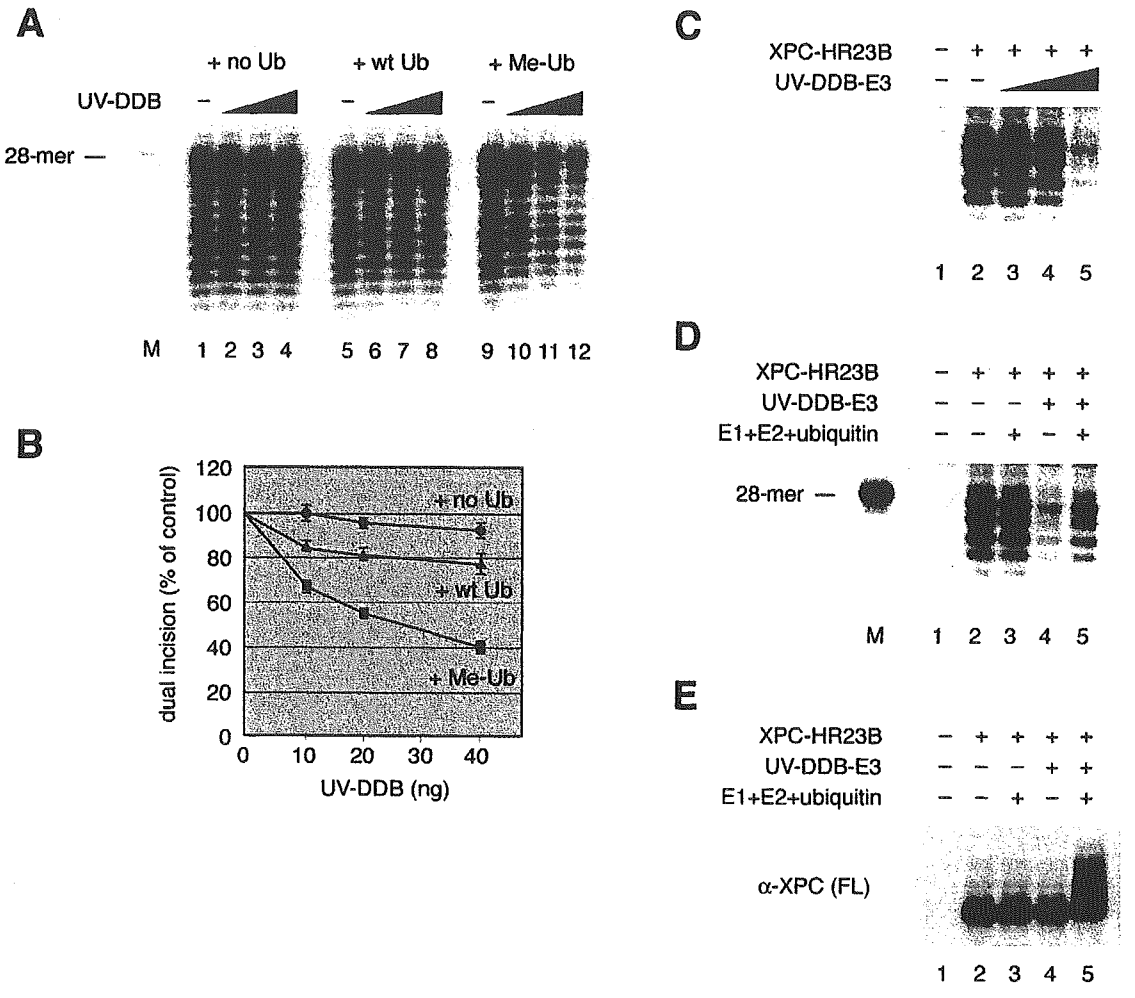

Figure 6. Effect of Ubiquitylation on Cell-Free NER Incision

(A) The internally ^{32}P-labeled DNA substrate containing a single 6-4PP was preincubated at 30°C for 10 min with various amounts of UV-DDB (FLAG-DDB1/DDB2 heterodimer; 10, 20, and 40 ng). The cell-free NER incision assay was then performed by adding the XP-E cell extract (100 μg protein) with or without 20 μg each of wild-type ubiquitin (wt Ub) or methylated ubiquitin (Me-Ub). Dual incision products detected on denaturing PAGE are shown. M, ^{32}P-labeled 28-mer oligonucleotide as a size marker (also for [D]).

(B) The levels of dual incision products for each lane in (A) were quantified, normalized relative to the value of the control reactions without UV-DDB, and plotted as a graph. The mean ± standard error of the mean was calculated from two independent experiments.

(C) Cell-free NER incision reactions were reconstituted with purified protein factors and carried out with the internally ^{32}P-labeled DNA substrate containing a single 6-4PP. Various amounts of purified UV-DDB-E3 (0.4, 4, and 40 ng) were also included (lanes 3–5). As a negative control, XPC-HR23B was omitted from the standard reaction (lane 1).

(D) Cell-free NER incision reactions were carried out with purified NER proteins in the presence or absence of UV-DDB-E3 (40 ng) and other factors required for ubiquitylation as indicated.

(E) The same set of reactions was carried out as described in (D), except that the unlabeled DNA substrate containing a 6-4PP was used. Aliquots of the reactions were subjected to immunoblotting with the anti-XPC (FL) antibody.

not shown). From a quantitative immunoblot analysis, we estimated that no more than 0.5 μg of endogenous, unconjugated ubiquitin was present in the extract included in a reaction (data not shown). Therefore, it was likely that the addition of K-less or methylated ubiquitin in such a large excess may competitively block the elongation of polyubiquitin chains. Immunoblot analyses revealed that UV-DDB-dependent polyubiquitylation of XPC indeed occurred in the NER reaction using the crude extract and that this was inhibited by the addition of K-less ubiquitin (Figure S5). The above results thus suggest that, when UV-DDB is bound to 6-4PP, the formation of relatively long polyubiquitin chains is important for subsequent processing of the lesion by NER. Similar experiments were carried out with a DNA substrate containing CPD instead of 6-4PP. In agreement with the previous report (Wakasugi et al., 2001), preincubation of the CPD substrate with UV-DDB resulted in a weak but detectable stimulation of dual incision in the XP-E cell extract, although quite large amounts of UV-DDB were required (Figure S6). In the presence of methylated ubiquitin, some stimulation by UV-DDB could still be observed.

To examine the direct involvement of ubiquitylation in

NER, we set up the reconstituted NER reaction with purified proteins. By using six purified essential NER factors (i.e., XPC-HR23B-centrin 2, XPA, XPF-ERCC1, XPG, transcription factor IIH [TFIIH], and replication protein A [RPA]), a significant level of dual incision could be detected with the internally radiolabeled 6-4PP substrate (Figure 6C, lane 2). The addition of the UV-DDB-E3 complex resulted in dose-dependent inhibition of the dual incision (lanes 3–5) if other ubiquitylating factors (E1, E2, and ubiquitin) were not present. Although the involvement of the ubiquitylating factors had little effect on the repair of 6-4PP (Figure 6D, lane 3), the inhibition caused by the UV-DDB-E3 complex appeared to be relieved at least partially in the presence of these factors (Figure 6D, compare lanes 4 and 5). The ubiquitylation of XPC under these reaction conditions was confirmed by immunoblotting (Figure 6E). In this reaction system, the efficiency of incision around CPD was too low to be detected. These results indicate that the elongation of polyubiquitin chains is important for NER of 6-4PP when UV-DDB is bound to the lesion.

Discussion

UV-DDB-Dependent Ubiquitylation of XPC

We have shown that the XPC protein is ubiquitylated in response to the UV irradiation of cells and that this ubiquitylation requires functional UV-DDB activity. It has been shown recently that UV-DDB associates in vivo with cullin 4A, Roc1, and COP9 signalosome, which suggests that this supercomplex may function as the E3 ligase complex (Groisman et al., 2003). The autoubiquitylation of cullin 4A subunit was indeed detected, but the physiological substrates of this E3 activity were not identified. Therefore, XPC is the first example of such an E3 substrate. This observation links the two known NER damage recognition factors and suggests a mechanism by which they operate together in NER.

Our present study demonstrates a direct physical interaction between XPC and UV-DDB that appears to be present even in unirradiated cells (Figure 3A). Moreover, in the absence of UV damage, the cullin 4A protein in the UV-DDB-E3 complex is not conjugated to Nedd8 (Groisman et al., 2003). This strongly suggests that the E3 may be inactivated through its association with the COP9 signalosome, which explains why XPC ubiquitylation is absent in unirradiated cells (Figure 7). However, when cells are irradiated with UV, UV-DDB-E3 translocates onto chromatin probably through its ability to interact with UV photolesions. Neddylated cullin 4A has been specifically detected in the chromatin bound fraction of UV-irradiated cells (Groisman et al., 2003). This suggests that the E3 associated with UV-DDB may be activated only when bound to UV-damaged chromatin. This also suggests that the ubiquitylation of XPC may occur exclusively on the damaged DNA (Figure 7). In our cell-free system, the addition of damaged DNA was not necessary for XPC ubiquitylation. This is not surprising, because we used the recombinant UV-DDB-E3 complex that lacks the COP9 signalosome and is thus constitutively active. For the two XP-E cell lines used in this study (XP2ROSV and XP82TO), mutations in the *DDB2* gene leads to inactivation of UV-DDB (Nichols et al., 1996). This suggests that, in these cells, E3 may never be activated even after UV irradiation. In contrast, XPC is normally ubiquitylated in XP-A, -B, -D, -F, and -G cells (Figure 2A). These observations indicate that XPC ubiquitylation may depend solely on the presence of functional UV-DDB and not on subsequent steps in the NER pathway.

Although our UV-DDB-associated recombinant E3 complex was active in the absence of DNA (Figure 4), its activity seemed to be further stimulated by the presence of 6-4PP (Figure 5A). This strongly suggests that the binding of UV-DDB to the lesion may affect the activity of UV-DDB-associated E3. Unlike the effect of UV irradiation, XPC ubiquitylation was much less pronounced when cells were treated with chemicals such as 4-NQO (Figure S1). This may be related to the observation that UV-DDB poorly recognizes 4-NQO-induced lesions (Payne and Chu, 1994). We also found that the binding affinities of UV-DDB for bubble and loop structures are far lower than that for 6-4PP (Figure S4C). This suggests that UV-DDB is not a versatile damage recognition factor like XPC; rather, it specializes in recognizing UV lesions, particularly 6-4PP. Such biochemical properties of UV-DDB may explain why exposure to UV but not the chemical carcinogen 7,12-dimethylbenz-[a]anthracene induced skin tumors in *DDB2*-deficient mice (Itoh et al., 2004). Taken together, it appears that the activation of E3 and the consequent ubiquitylation of XPC are not associated with all GG-NER lesions; rather, the occurrence of these events depends on the binding affinity of UV-DDB for the induced lesions.

Roles of Ubiquitylation in GG-NER

Although XPC acquired polyubiquitin chains in our cell-free system, the UV-induced modification of XPC appeared to be reversible and did not induce degradation via the 26S proteasome. Mechanisms that protect the ubiquitylated XPC from degradation thus may exist. In regard to this, it has been noted that complex formation with HR23 proteins stabilizes XPC (Ng et al., 2003; Okuda et al., 2004), perhaps because this regulates its degradation via the ubiquitin/proteasome pathway. Notably, the UV-DDB-E3 complex also ubiquitylated two of its own subunits in vitro, namely DDB2 and cullin 4A. As reported previously (Fitch et al., 2003a; Rapic'-Otrin et al., 2002), DDB2 appeared to be degraded after UV irradiation (Figure S3). Thus, the fates of ubiquitylated XPC and DDB2 appear to be quite different, even though the two proteins are probably ubiquitylated by the same E3 molecules.

The DDB1/DDB2 heterodimer binds to 6-4PP with very high affinity and specificity (Fujiwara et al., 1999; Reardon et al., 1993; Treiber et al., 1992). Since the binding affinity of XPC for this lesion is much lower (Figure S4) and UV-DDB rapidly translocates into the locally irradiated area in the nucleus without functional XPC (Wakasugi et al., 2002), UV-DDB is probably the first NER factor to recognize and bind 6-4PP in vivo. Notably, although the addition of UV-DDB inhibited our NER reactions that were reconstituted with six purified essential proteins (Figure 6C), the reactions using the XP-E cell extract appeared to be much more resistant

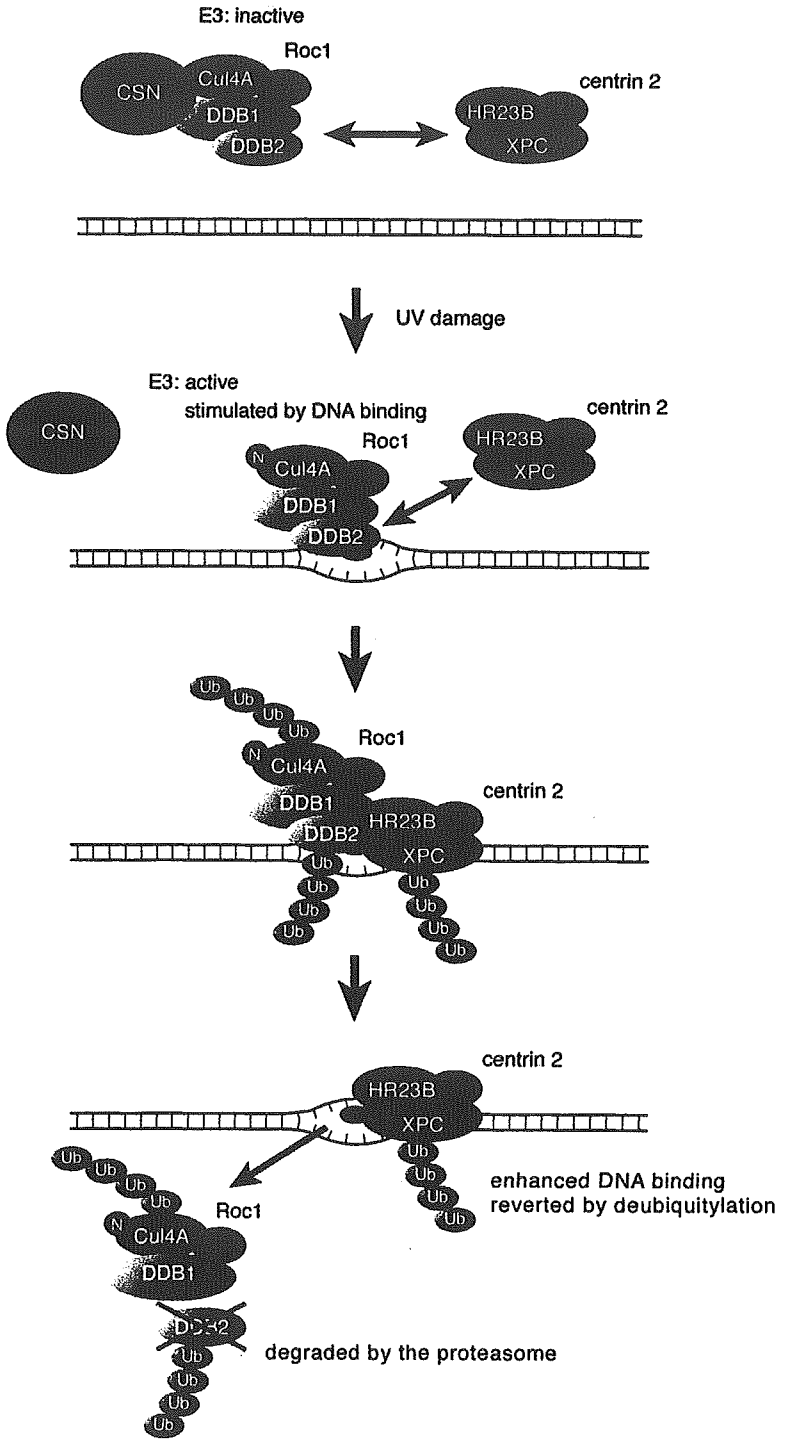

Figure 7. Model for UV-Induced UV-DDB-Dependent Ubiquitylation of XPC

In unirradiated cells, UV-DDB-associated E3 is inactivated by its interaction with the COP9 signalosome (CSN). Thus, XPC is not ubiquitylated, despite its interaction with UV-DDB. Upon UV irradiation, UV-DDB translocates onto the damaged chromatin by binding to lesions, particularly 6-4PP. Its dissociation from the CSN and the neddylation of cullin 4A (indicated by "N") activate E3. The binding of UV-DDB to the lesion further stimulates E3 activity. The activated UV-DDB-E3 then recruits XPC via protein-protein interaction, and XPC, DDB2, and cullin 4A are ubiquitylated at the lesion site. Polyubiquitylated UV-DDB loses its damaged DNA binding activity, whereas the DNA binding of XPC is potentiated by its ubiquitylation. This results in the displacement of UV-DDB by XPC on the lesion. The ubiquitylated DDB2 is degraded by the proteasome. The ubiquitylated form of XPC reverts to the unmodified form through deubiquitylation.

to UV-DDB (Figure 6A), which strongly suggests that specific factors are required for the repair of 6-4PP in the presence of UV-DDB. One can imagine that the extremely stable binding of UV-DDB to 6-4PP could prevent the subsequent binding of other GG-NER factors, including XPC. Based on our present results, we propose that UV-DDB-dependent polyubiquitylation is involved in the displacement of UV-DDB by XPC from 6-4PP (Figure 7). The evidence for this notion is as follows. First, UV-DDB appears to lose its high binding affinity for 6-4PP when DDB2 is extensively polyubiquitylated, whereas XPC polyubiquitylated under the same conditions displayed a higher DNA binding activity compared to its unmodified form (Figure 5). These alterations in DNA binding properties would certainly aid the replacement of UV-DDB by XPC. Second, the inhibition

of polyubiquitin chain elongation by adding K-less or methylated ubiquitin revealed the UV-DDB-dependent inhibition of 6-4PP repair in the XP-E cell extract (Figures 6A and 6B). Finally, the addition of the ubiquitylation factors to the reconstituted NER reaction removed the UV-DDB-dependent inhibition of 6-4PP repair (Figure 6D), although the incision activity was only partially restored under the conditions tested. This might be explained by the relatively unstable association of E3 in our preparation of the UV-DDB complex (Figure 5A), since UV-DDB that has lost E3 probably inhibits the repair of 6-4PP. Moreover, the reconstituted NER reaction may still be missing additional factors that are present in the crude cell extract and are specifically required when UV-DDB-dependent ubiquitylation occurs.

In XP-E cells lacking UV-DDB, GG-NER of 6-4PP is almost normal, even though UV-induced ubiquitylation of XPC is absent. The above model is consistent with this phenotype of XP-E cells, because it indicates that XPC ubiquitylation is only required when UV-DDB is present, since XPC is able to detect 6-4PP by itself without ubiquitylation. Notably, NER functions of UV-DDB have been documented mainly in connection with the repair of CPD rather than 6-4PP (Hwang et al., 1999; Tang et al., 2000). We have previously shown that the XPC complex by itself recognizes CPD very poorly, presumably because the distortion of the helix induced by the lesion is too small (Sugasawa et al., 2001). For such lesions, recognition by UV-DDB may facilitate the recruitment of other NER factors including XPC (Fitch et al., 2003b). From our in vitro experiments, the involvement of UV-DDB-dependent ubiquitylation in CPD repair was not clear, since stimulation of CPD repair by UV-DDB still appeared to occur in the absence of polyubiquitylation (Figure S6). However, the observed stimulation was nonetheless quite weak and required unphysiologically high concentrations of UV-DDB. This raises the possibility that even the in vitro NER reaction using the crude cell extract may require optimization before the precise roles of UV-DDB and ubiquitylation in CPD repair can be examined. However, since UV-DDB appears, upon extensive polyubiquitylation, to lose its binding activity to not only 6-4PP but also CPD (Figure 5A), it cannot be excluded that ubiquitylation may also be associated with CPD repair.

Given that XPC is able to recognize 6-4PP by itself, what is the biological significance of such a high binding affinity of UV-DDB for 6-4PP? Although many published studies indicate that the lack of UV-DDB barely affects the efficiency with which 6-4PP is repaired in vivo, it has been shown very recently that UV-DDB can facilitate the recruitment of XPC as well as other NER factors to sites containing 6-4PP, particularly when the number of induced 6-4PP lesions is relatively low (L.H.F. Mullenders, personal communication). We favor the idea that UV-DDB is involved in efficiently recruiting XPC to UV lesions, regardless of whether these lesions are CPD or 6-4PP, since this supports the biological relevance of our in vitro results that point to the roles ubiquitylation plays in the repair of 6-4PP. As proposed in Figure 7, one of the roles UV-induced XPC ubiquitylation may play is that it reinforces the DNA binding of XPC, which helps displace UV-DDB from the lesion (even though UV-DDB initially binds to the UV lesion more strongly than XPC). These observations together appear to add quite novel insights into the damage recognition mechanisms involved in DNA repair, as well as to the functions of ubiquitylation. However, it cannot be excluded that the ubiquitylation of XPC and UV-DDB may play additional roles. For instance, polyubiquitylated XPC and/or DDB2 may be involved in signal transduction pathways that are activated in response to DNA damage. In addition, the degradation of DDB2 itself may serve as a certain intracellular signal. To fully understand the roles of UV-DDB-dependent ubiquitylation, it would be of great interest to generate mutant XPC and DDB2 molecules that specifically lack their interaction or ubiquitylation sites. In addition, it would be highly informative to identify the factors that interact specifically with ubiquitylated XPC and/or UV-DDB.

Experimental Procedures

Additional information can be found in the Supplemental Data.

Cell Lines and Cultures

WI38 VA13 cells as well as other human fibroblast cell lines derived from XP and CS patients were cultured at 37°C in Dulbecco's modified Eagle's medium containing 10% fetal bovine serum. Chinese hamster cells were cultured under the same conditions, except for the addition of L-proline with CHO-K1 cells. Stable V79 transformants expressing human DDB2 were established as described previously (Tang et al., 2000) and cultured in the presence of 500 μg/ml G418 (Invitrogen). A lymphoblastoid cell line (GM01646) from an XP-E patient was obtained from the Coriell Cell Repository and cultured in suspension with RPMI1640 medium containing 15% heat-inactivated fetal bovine serum. Mouse mammary carcinoma FM3A as well as its temperature-sensitive mutant ts85 cells were maintained at 33°C in suspension with RPMI1640 medium containing 10% calf serum.

Purified Protein Factors

Human XPC and His_6-tagged HR23B (HR23B-His) proteins were expressed and purified separately as described previously (Sugasawa et al., 2001). In vitro reconstitution of the XPC-HR23B-His heterodimer has also been described previously (Sugasawa et al., 2001). Centrin 2 was expressed in *E. coli* and purified as described (Araki et al., 2001).

Other NER factors except TFIIH were expressed in insect cells by using the baculovirus system. Detailed purification procedures are given in the Supplemental Data. The human TFIIH complex was purchased from ProteinOne. Rabbit E1 and human UbcH5a (E2) enzymes as well as ubiquitin (wild-type, K-less, or GST-tagged) were purchased from Boston Biochem, while wild-type ubiquitin was also obtained from Sigma.

In Vitro Ubiquitylation Assay

The standard reaction mixture (15 μl) contained 50 mM Tris-HCl (pH 7.6), 10 mM $MgCl_2$, 0.2 mM $CaCl_2$, 4 mM ATP, 1 mM dithiothreitol (DTT), bovine serum albumin (BSA; 1.5 μg), E1 (0.1 μg), E2 (0.4 μg), ubiquitin (5 μg), purified UV-DDB-E3 (20 ng), and XPC-HR23B-His. The reactions were incubated at 37°C for 1 hr, stopped by adding 1 μl of 0.5 M EDTA, and subjected to SDS-PAGE followed by immunoblot analyses using appropriate antibodies.

Damaged DNA Binding Assay

Details of DNA bead preparation are provided in the Supplemental Data. Binding reactions were performed at 30°C for 30 min in mixtures (15 μl) containing 50 mM Tris-HCl (pH 7.6), 5 mM $MgCl_2$, 0.2 mM $CaCl_2$, 2 mM ATP, 1 mM DTT, 0.1 M NaCl, BSA (1.5 μg), varied amounts of XPC-HR23B-His (together with a four times molar excess of centrin 2), and 12 μg of the paramagnetic beads containing 1 pmol of UV lesions or the corresponding amount of undamaged DNA as a control. Where indicated, UV-DDB-E3 (20 ng), E1 (0.1 μg), E2 (0.5 μg), and ubiquitin (wild-type or methylated; 10 μg) were

also included. After the reactions were stopped by adding 1 μl of 0.5 M EDTA, the supernatants were saved as "unbound" fractions. The beads were then washed twice with 50 μl of ice-cold wash buffer (50 mM Tris-HCl [pH 7.6], 5 mM $MgCl_2$, 0.2 mM $CaCl_2$, 0.1 M NaCl, 1 mM DTT) and suspended in SDS sample buffer. Aliquots of the unbound and bound fractions were subjected to SDS-PAGE followed by immunoblotting.

NER Dual Incision Assay

The internally ^{32}P-labeled, double-stranded circular DNA substrate that contains a single, site-specific 6-4PP or CPD, and whole-cell extract from the XP-E lymphoblastoid cells (GM01646) were prepared as described previously (Sugasawa et al., 2001). The standard reaction mixture (25 μl) contained 40 mM Hepes-KOH (pH 7.8), 5 mM $MgCl_2$, 2 mM ATP, 0.5 mM DTT, 70 mM NaCl, 5% glycerol, BSA (5.4 μg), the XP-E cell extract (100 μg of protein), 22.5 mM creatine phosphate (di-Tris; Sigma), creatine phosphokinase (0.5 μg; Sigma type I), and the ^{32}P-labeled DNA substrate (~1 × 10^5 cpm for 6-4PP and ~4 × 10^5 cpm for CPD, respectively). For the reconstituted NER, the reaction volume was reduced to 15 μl; the XP-E cell extract was replaced by FLAG-XPA (25 ng), RPA (100 ng), XPF-ERCC1-His (12 ng), XPG (12 ng), TFIIH (134 ng), XPC-HR23B-His (20 ng), and centrin 2 (5 ng); and the NaCl concentration was adjusted at 100 mM. Where indicated, E1 (0.1 μg), E2 (0.5 μg), ubiquitin (wild-type, K-less, or methylated), and varied amounts of UV-DDB or UV-DDB-E3 complex were also included. After incubation at 30°C for 1 hr, the DNA was purified and subjected to 10% denaturing PAGE followed by autoradiography.

Supplemental Data

Supplemental Data include six figures, Supplemental Experimental Procedures, and Supplemental References and can be found with this article online at http://www.cell.com/cgi/content/full/121/3/387/DC1/.

Acknowledgments

We thank all the members of the Cellular Physiology Laboratory for helpful discussions and encouragement. We also thank M. Yamaizumi (Kumamoto University) for the XP82TO cells, A. Shimamoto (GeneCare Research Institute Co. Ltd.) for cDNA encoding HA-tagged ubiquitin, and Y. Saeki (University of Tokyo) for helpful discussions. This work was supported by grants from the Ministry of Education, Culture, Sports, Science and Technology of Japan and from the Human Frontier Science Program and by the Core Research for Evolutional Science and Technology (CREST) from the Japan Science and Technology Agency. This work was also supported by the Bioarchitect Research Project and the Chemical Biology Research Project of RIKEN.

Received: July 30, 2004
Revised: November 18, 2004
Accepted: February 20, 2005
Published: May 5, 2005

References

Aboussekhra, A., Biggerstaff, M., Shivji, M.K.K., Vilpo, J.A., Moncollin, V., Podust, V.N., Protic, M., Hübscher, U., Egly, J.-M., and Wood, R.D. (1995). Mammalian DNA nucleotide excision repair reconstituted with purified protein components. Cell *80*, 859–868.

Araki, M., Masutani, C., Takemura, M., Uchida, A., Sugasawa, K., Kondoh, J., Ohkuma, Y., and Hanaoka, F. (2001). Centrosome protein centrin 2/caltractin 1 is part of the xeroderma pigmentosum group C complex that initiates global genome nucleotide excision repair. J. Biol. Chem. *276*, 18665–18672.

Araújo, S.J., Tirode, F., Coin, F., Pospiech, H., Syväoja, J.E., Stucki, M., Hübscher, U., Egly, J.-M., and Wood, R.D. (2000). Nucleotide excision repair of DNA with recombinant human proteins: definition of the minimal set of factors, active forms of TFIIH, and modulation by CAK. Genes Dev. *14*, 349–359.

Batty, D., Rapic'-Otrin, V., Levine, A.S., and Wood, R.D. (2000). Stable binding of human XPC complex to irradiated DNA confers strong discrimination for damaged sites. J. Mol. Biol. *300*, 275–290.

Bootsma, D., Kraemer, K.H., Cleaver, J.E., and Hoeijmakers, J.H.J. (1997). Nucleotide excision repair syndromes: xeroderma pigmentosum, Cockayne syndrome, and trichothiodystrophy. In The Metabolic Basis of Inherited Disease, C.R. Scriver, A.L. Beaudet, W.S. Sly, and D. Valle, eds. (New York: McGraw-Hill Book Co.), pp. 245–274.

Chu, G., and Chang, E. (1988). Xeroderma pigmentosum group E cells lack a nuclear factor that binds to damaged DNA. Science *242*, 564–567.

Finley, D., Ciechanover, A., and Varshavsky, A. (1984). Thermolability of ubiquitin-activating enzyme from the mammalian cell cycle mutant ts85. Cell *37*, 43–55.

Fitch, M.E., Cross, I.V., Turner, S.J., Adimoolam, S., Lin, C.X., Williams, K.G., and Ford, J.M. (2003a). The DDB2 nucleotide excision repair gene product p48 enhances global genomic repair in p53 deficient human fibroblasts. DNA Repair (Amst.) *2*, 819–826.

Fitch, M.E., Nakajima, S., Yasui, A., and Ford, J.M. (2003b). In vivo recruitment of XPC to UV-induced cyclobutane pyrimidine dimers by the DDB2 gene product. J. Biol. Chem. *278*, 46906–46910.

Friedberg, E.C. (2001). How nucleotide excision repair protects against cancer. Nat. Rev. Cancer *1*, 22–33.

Fujiwara, Y., Masutani, C., Mizukoshi, T., Kondo, J., Hanaoka, F., and Iwai, S. (1999). Characterization of DNA recognition by the human UV-damaged DNA-binding protein. J. Biol. Chem. *274*, 20027–20033.

Groisman, R., Polanowska, J., Kuraoka, I., Sawada, J., Saijo, M., Drapkin, R., Kisselev, A.F., Tanaka, K., and Nakatani, Y. (2003). The ubiquitin ligase activity in the DDB2 and CSA complexes is differentially regulated by the COP9 signalosome in response to DNA damage. Cell *113*, 357–367.

Hoeijmakers, J.H.J. (2001). Genome maintenance mechanisms for preventing cancer. Nature *411*, 366–374.

Hwang, B.J., Toering, S., Francke, U., and Chu, G. (1998). p48 activates a UV-damaged DNA-binding factor and is defective in xeroderma pigmentosum group E cells that lack binding activity. Mol. Cell. Biol. *18*, 4391–4399.

Hwang, B.J., Ford, J.M., Hanawalt, P.C., and Chu, G. (1999). Expression of the p48 xeroderma pigmentosum gene is p53 dependent and is involved in global genome repair. Proc. Natl. Acad. Sci. USA *96*, 424–428.

Itoh, T., Linn, S., Ono, T., and Yamaizumi, M. (2000). Reinvestigation of the classification of five cell strains of xeroderma pigmentosum group E with reclassification of three of them. J. Invest. Dermatol. *114*, 1022–1029.

Itoh, T., Cado, D., Kamide, R., and Linn, S. (2004). DDB2 gene disruption leads to skin tumors and resistance to apoptosis after exposure to ultraviolet light but not a chemical carcinogen. Proc. Natl. Acad. Sci. USA *101*, 2052–2057.

Masutani, C., Sugasawa, K., Yanagisawa, J., Sonoyama, T., Ui, M., Enomoto, T., Takio, K., Tanaka, K., van der Spek, P.J., Bootsma, D., et al. (1994). Purification and cloning of a nucleotide excision repair complex involving the xeroderma pigmentosum group C protein and a human homolog of yeast RAD23. EMBO J. *13*, 1831–1843.

Matsumoto, Y., Yasuda, H., Marunouchi, T., and Yamada, M. (1983). Decrease in uH2A (protein A24) of a mouse temperature-sensitive mutant. FEBS Lett. *151*, 139–142.

Mu, D., Park, C.H., Matsunaga, T., Hsu, D.S., Reardon, J.T., and Sancar, A. (1995). Reconstitution of human DNA repair excision nuclease in a highly defined system. J. Biol. Chem. *270*, 2415–2418.

Ng, J.M.Y., Vermeulen, W., van der Horst, G.T.J., Bergink, S., Sugasawa, K., Vrieling, H., and Hoeijmakers, J.H.J. (2003). A novel regulation mechanism of DNA repair by damage-induced and RAD23-dependent stabilization of xeroderma pigmentosum group C protein. Genes Dev. *17*, 1630–1645.

Nichols, A.F., Ong, P., and Linn, S. (1996). Mutations specific to the xeroderma pigmentosum group E Ddb- phenotype. J. Biol. Chem. *271*, 24317–24320.

Okuda, Y., Nishi, R., Ng, J.M.Y., Vermeulen, W., van der Horst, G.T.J., Mori, T., Hoeijmakers, J.H.J., Hanaoka, F., and Sugasawa, K. (2004). Relative levels of the two mammalian Rad23 homologs determine composition and stability of the xeroderma pigmentosum group C protein complex. DNA Repair (Amst.) *3*, 1285–1295.

Otrin, V.R., McLenigan, M., Takao, M., Levine, A.S., and Protic, M. (1997). Translocation of a UV-damaged DNA binding protein into a tight association with chromatin after treatment of mammalian cells with UV light. J. Cell Sci. *110*, 1159–1168.

Payne, A., and Chu, G. (1994). Xeroderma pigmentosum group E binding factor recognizes a broad spectrum of DNA damage. Mutat. Res. *310*, 89–102.

Rapic'-Otrin, V., McLenigan, M.P., Bisi, D.C., Gonzalez, M., and Levine, A.S. (2002). Sequential binding of UV DNA damage binding factor and degradation of the p48 subunit as early events after UV irradiation. Nucleic Acids Res. *30*, 2588–2598.

Rapic'-Otrin, V., Navazza, V., Nardo, T., Botta, E., McLenigan, M., Bisi, D.C., Levine, A.S., and Stefanini, M. (2003). True XP group E patients have a defective UV-damaged DNA binding protein complex and mutations in DDB2 which reveal the functional domains of its p48 product. Hum. Mol. Genet. *12*, 1507–1522.

Reardon, J.T., Nichols, A.F., Keeney, S., Smith, C.A., Taylor, J.S., Linn, S., and Sancar, A. (1993). Comparative analysis of binding of human damaged DNA-binding protein (XPE) and *Escherichia coli* damage recognition protein (UvrA) to the major ultraviolet photoproducts: T[c,s]T, T[t,s]T, T[6-4]T, and T[Dewar]T. J. Biol. Chem. *268*, 21301–21308.

Riedl, T., Hanaoka, F., and Egly, J.-M. (2003). The comings and goings of nucleotide excision repair factors on damaged DNA. EMBO J. *22*, 5293–5303.

Shivji, M.K.K., Eker, A.P.M., and Wood, R.D. (1994). DNA repair defect in xeroderma pigmentosum group C and complementing factor from HeLa cells. J. Biol. Chem. *269*, 22749–22757.

Sugasawa, K., Ng, J.M.Y., Masutani, C., Iwai, S., van der Spek, P.J., Eker, A.P.M., Hanaoka, F., Bootsma, D., and Hoeijmakers, J.H.J. (1998). Xeroderma pigmentosum group C protein complex is the initiator of global genome nucleotide excision repair. Mol. Cell *2*, 223–232.

Sugasawa, K., Okamoto, T., Shimizu, Y., Masutani, C., Iwai, S., and Hanaoka, F. (2001). A multistep damage recognition mechanism for global genomic nucleotide excision repair. Genes Dev. *15*, 507–521.

Sugasawa, K., Shimizu, Y., Iwai, S., and Hanaoka, F. (2002). A molecular mechanism for DNA damage recognition by the xeroderma pigmentosum group C protein complex. DNA Repair (Amst.) *1*, 95–107.

Tang, J.Y., Hwang, B.J., Ford, J.M., Hanawalt, P.C., and Chu, G. (2000). Xeroderma pigmentosum p48 gene enhances global genomic repair and suppresses UV-induced mutagenesis. Mol. Cell *5*, 737–744.

Tornaletti, S., and Hanawalt, P.C. (1999). Effect of DNA lesions on transcription elongation. Biochimie *81*, 139–146.

Treiber, D.K., Chen, Z., and Essigmann, J.M. (1992). An ultraviolet light-damaged DNA recognition protein absent in xeroderma pigmentosum group E cells binds selectively to pyrimidine (6-4) pyrimidone photoproducts. Nucleic Acids Res. *20*, 5805–5810.

Volker, M., Moné, M.J., Karmakar, P., van Hoffen, A., Schul, W., Vermeulen, W., Hoeijmakers, J.H.J., van Driel, R., van Zeeland, A.A., and Mullenders, L.H.F. (2001). Sequential assembly of the nucleotide excision repair factors in vivo. Mol. Cell *8*, 213–224.

Wakasugi, M., Shimizu, M., Morioka, H., Linn, S., Nikaido, O., and Matsunaga, T. (2001). Damaged DNA-binding protein DDB stimulates the excision of cyclobutane pyrimidine dimers in vitro in concert with XPA and replication protein A. J. Biol. Chem. *276*, 15434–15440.

Wakasugi, M., Kawashima, A., Morioka, H., Linn, S., Sancar, A., Mori, T., Nikaido, O., and Matsunaga, T. (2002). DDB accumulates at DNA damage sites immediately after UV irradiation and directly stimulates nucleotide excision repair. J. Biol. Chem. *277*, 1637–1640.

Impairment of starvation-induced and constitutive autophagy in *Atg7*-deficient mice

Masaaki Komatsu,[1,3] Satoshi Waguri,[2] Takashi Ueno,[3] Junichi Iwata,[3] Shigeo Murata,[1] Isei Tanida,[3] Junji Ezaki,[3] Noboru Mizushima,[4] Yoshinori Ohsumi,[5] Yasuo Uchiyama,[2] Eiki Kominami,[3] Keiji Tanaka,[1] and Tomoki Chiba[1]

[1]Department of Molecular Oncology, Tokyo Metropolitan Institute of Medical Science, Bunkyo-ku, Tokyo 113-8613, Japan
[2]Department of Cell Biology and Neurosciences, Osaka University Graduate School of Medicine, Osaka 565-0871, Japan
[3]Department of Biochemistry, Juntendo University School of Medicine, Bunkyo-ku, Tokyo 113-8421, Japan
[4]Department of Bioregulation and Metabolism, Tokyo Metropolitan Institute of Medical Science, Bunkyo-ku, Tokyo 113-8613, Japan
[5]Department of Cell Biology, National Institute for Basic Biology, Okazaki 444-8585, Japan

Autophagy is a membrane-trafficking mechanism that delivers cytoplasmic constituents into the lysosome/vacuole for bulk protein degradation. This mechanism is involved in the preservation of nutrients under starvation condition as well as the normal turnover of cytoplasmic component. Aberrant autophagy has been reported in several neurodegenerative disorders, hepatitis, and myopathies. Here, we generated conditional knockout mice of *Atg7*, an essential gene for autophagy in yeast. *Atg7* was essential for ATG conjugation systems and autophagosome formation, amino acid supply in neonates, and starvation-induced bulk degradation of proteins and organelles in mice. Furthermore, *Atg7* deficiency led to multiple cellular abnormalities, such as appearance of concentric membranous structure and deformed mitochondria, and accumulation of ubiquitin-positive aggregates. Our results indicate the important role of autophagy in starvation response and the quality control of proteins and organelles in quiescent cells.

Introduction

There are two major protein degradation pathways in eukaryotic cells: the proteasome and the lysosome. The proteasome is a self-compartmentalized protease complex with catalytic activities inside its central proteinaceous chamber (Baumeister et al., 1998). It plays crucial roles in selective degradation of not only short-lived regulatory proteins but also abnormal proteins that should be eliminated from the cells (Goldberg, 2003). In contrast, the lysosome is a vesicle that contains many hydrolases, which are separated from the cytosol by the limiting membrane. In this lysosomal pathway, degradation of plasma membrane proteins and extracellular proteins is mediated by endocytosis, whereas degradation of cytoplasmic components is achieved through several pathways: macroautophagy, microautophagy, and chaperone-mediated autophagy (Seglen and Bohley, 1992; Dunn, 1994; Klionsky and Emr, 2000; Massey et al., 2004).

Macroautophagy (hereafter referred to as autophagy) is the main route for sequestration of the cytoplasm into the lysosome. The initial step of autophagy is elongation of the isolation membrane. The isolation membrane initially enwraps cytoplasmic constituents such as organelles, and then its edges fuse with each other forming a double membrane structure called autophagosome. Finally, the outer membrane of the autophagosome fuses with the lysosome/vacuole and the sequestered cytoplasmic components are degraded by the lysosomal/vacuolar hydrolases, together with the inner membrane of the autophagosomes (Mizushima et al., 2002).

In mammals, autophagy is considered necessary for the turnover of cellular components, particularly in response to starvation or glucagons (Mortimore and Poso, 1987). Yeast deficient in autophagy rapidly die under nutrition-poor conditions (Tsukada and Ohsumi, 1993), suggesting its important roles in preservation of nutrient supply. Indeed, autophagy is necessary for survival in early neonatal starvation period in mice (Kuma et al., 2004). Furthermore, autophagy plays a role in cellular remodeling during differentiation and development of multicellular organisms, such as fly, worm, and slime mold (Levine and Klionsky, 2004), and cellular defense against invading streptococcus (Nakagawa et al., 2004). Plants deficient in autophagy show accelerated senescence (Hanaoka et al., 2002). In humans, autophagy has been implicated in several pathological conditions (Shintani and Klionsky, 2004); e.g., low levels of autophagy were described in some malignant tumors (Liang et al., 1999).

Correspondence to Tomoki Chiba: tchiba@rinshoken.or.jp

Abbreviations used in this paper: MEF, mouse embryonic fibroblast; plpC, polyinosinic acid–polycytidylic acid; PNS, postnuclear supernatant; SDH, succinate dehydrogenase.

The online version of this article includes supplemental material.

The Journal of Cell Biology, Vol. 169, No. 3, May 9, 2005 425–434
http://www.jcb.org/cgi/doi/10.1083/jcb.200412022

In contrast, elevated levels of autophagosome formation were reported in other human pathologies such as neurodegenerative diseases, myopathies, and liver injury (Mizushima et al., 2002; Perlmutter, 2002), and autophagy is implicated in the execution of cell death (Xue et al., 1999; Bursch, 2001). However, the high level of autophagosome formation does not necessarily reflect enhanced protein degradation because the formation of autophagosomes is increased in Danon cardiomyopathy, which is characterized by defective lysosomal degradation (Nishino et al., 2000; Tanaka et al., 2000). Thus, it is not clear whether increased levels of autophagosome formation reflect the activation or defective protein degradation.

Although autophagy has been extensively studied, little was known about its molecular mechanism until the recent discovery of *ATG* genes in budding yeast (Tsukada and Ohsumi, 1993). Of the many *ATG* genes, seven uniquely compose two ubiquitin-like conjugation systems: ATG12 and ATG8 conjugation systems (Mizushima et al., 1998; Ichimura et al., 2000; Ohsumi, 2001). The ubiquitin-like protein Atg12p covalently attaches to Atg5p in a reaction similar to ubiquitination. In this process, Atg12p is activated by an E1-like enzyme, Atg7p (Tanida et al., 1999), and transferred to an E2-like enzyme, Atg10p (Shintani et al., 1999), and then finally conjugates to Atg5p. Atg8p, another ubiquitin-like protein, is unique among other ubiquitin-like molecules, as it conjugates to phosphatidyl-ethanolamine (Ichimura et al., 2000). Atg8p is activated by Atg7p, which is common to the Atg12 conjugation system, and is transferred to Atg3p, an E2-like enzyme (Ichimura et al., 2000). In mammals, there exist at least three Atg8 homologues that can all be activated by Atg7 (Tanida et al., 2001), GATE-16, GABARAP, and LC3 (Ohsumi, 2001), and they localize to the autophagosome (Kabeya et al., 2000, 2004).

Here, we generated conditional knockout mice of *Atg7* and analyzed the roles of autophagy in neonates and adult liver. Autophagosome formation and starvation-induced degradation of proteins and organelles was impaired in *Atg7*-deficient mice and adult livers. We also found an important role for autophagy in constitutive turnover of cytoplasmic components, and its loss resulted in accumulation of abnormal organelles and ubiquitinated proteins. Our results suggest that autophagy is important for clearance of ubiquitin-positive aggregates.

Results

Generation of *Atg7* conditional knockout mice

To investigate the physiological roles of autophagy in mammals, we generated *Atg7* conditional knockout mice. Mouse *Atg7* gene is encoded by 17 exons that span 216-kb long genomic DNA. The active site cysteine residue essential for activation of the substrates is encoded by exon 14 and the targeting vector is designed to conditionally disrupt this exon by Cre-*loxP* technology. The targeted exon 14 was modified so that it could express Atg7 even in the presence of neo-resistant gene cassette in intron 14 (Fig. 1 A). Mice homozygous for the $Atg7^{Flox}$ allele (referred to as $Atg7^{F/F}$ mice), which were expected to express intact Atg7, were born healthy and fertile without any noticeable pathological phenotypes. Fig. 1 B shows Southern blots of mice with the indicated genotypes. Immunoblot analysis revealed the presence of Atg7 protein in $Atg7^{F/F}$ mouse embryonic fibroblasts (MEFs; Fig. 1 C), suggesting that Atg7 is efficiently expressed from the $Atg7^{Flox}$ allele.

The phenotype of *Atg7*-deficient mice

To examine the *Atg7*-deficient phenotype, we bred $Atg7^{F/F}$ mice with a line of transgenic mice that express the Cre recombinase under the control of the Zp3 promoter in the oocyte (Lewandoski et al., 1997). The heterozygous mice (referred to as $Atg7^{+/-}$) were obtained from female $Atg7^{F/+}$:Zp3 mice. $Atg7^{+/-}$ mice were born healthy and fertile without any noticeable pathological phenotypes for 1 yr. The $Atg7^{-/-}$ mice, obtained by breeding $Atg7^{+/-}$ mice, were born at Mendelian frequency (+/+: +/−: −/− = 21: 38: 19). The results of PCR genotyping are shown in Fig. 2 A. Neither Atg7 mRNA nor protein was detected in the homozygous mice (Fig. 2, B and C). We also tested the loss of Atg7 activity by examining the ATG conjugation systems in the neonate liver. A 56-kD protein, equivalent to Atg5–Atg12 conjugate, was detected by Atg5 antibody in the control $Atg7^{+/-}$ but not $Atg7^{-/-}$ liver (Fig. 2 C). In contrast, free Atg5 of 30 kD, which was faintly observed in the $Atg7^{+/-}$ liver, increased in $Atg7^{-/-}$ liver (Fig. 2 C). Mammalian Atg8p homologue LC3 has two forms (i.e., LC3-I and LC3-II; Kabeya et al., 2000). It is generally accepted that LC3-I is the free mature form whereas LC3-II is the lipidated form, in analogy to yeast Atg8p (Ichimura et al., 2000; Kabeya et al., 2000). Both forms were detected in $Atg7^{+/-}$ liver whereas only the LC3-I form was detected and increased in $Atg7^{-/-}$ liver (Fig. 2 C). When crossed with GFP-LC3 transgenic mice (Mizushima et al., 2004), the punctate structures representing autophagosomes were detected in $Atg7^{+/-}$ but not in $Atg7^{-/-}$ heart (Fig. 2, D and E). These results indicate that *Atg7* is essential for ATG conjugation systems and autophagosome formation in mice.

Although homozygous mice seemed normal at birth (Fig. 2 F) and had no apparent developmental defect by histological analyses (Fig. S1, available at http://www.jcb.org/cgi/content/full/jcb.200412022/DC1), the mean body weight of $Atg7^{-/-}$ mice (0.983 ± 0.0763 g, ± SD, $n = 9$) was significantly lower than that of wild-type and heterozygote mice (1.20 ± 0.116 g, $n = 29$; $P < 0.01$), and $Atg7^{-/-}$ mice died within 1 d after birth ($n = 19$). We considered that $Atg7^{-/-}$ mice could survive in utero by virtue of the nutrients supplied through the placenta but could not survive when the supply terminates after birth, as recently reported (Kuma et al., 2004). We tested the survival time of $Atg7^{-/-}$ neonates under starvation condition after caesarean delivery. Wild-type and heterozygous mice died at 21.7 ± 3.3 h after birth, whereas $Atg7^{-/-}$ mice died at 13 ± 2.0 h ($P < 0.01$; Fig. 2 G). To further test whether the cause of earlier death correlates with lower nutrient supply, we measured amino acid concentrations in plasma at 10 h after caesarean delivery. Essential and branched-chain amino acid concentrations in the sera of $Atg7^{-/-}$ mice were lower than those of wild-type mice (essential amino acids: 1.536 ± 0.087 vs. 1.291 ± 0.166 mmol/L, $P < 0.05$; branched-chain amino acids: 0.375 ± 0.038 vs. 0.268 ± 0.015 mmol/L, $P < 0.01$, respectively). The same

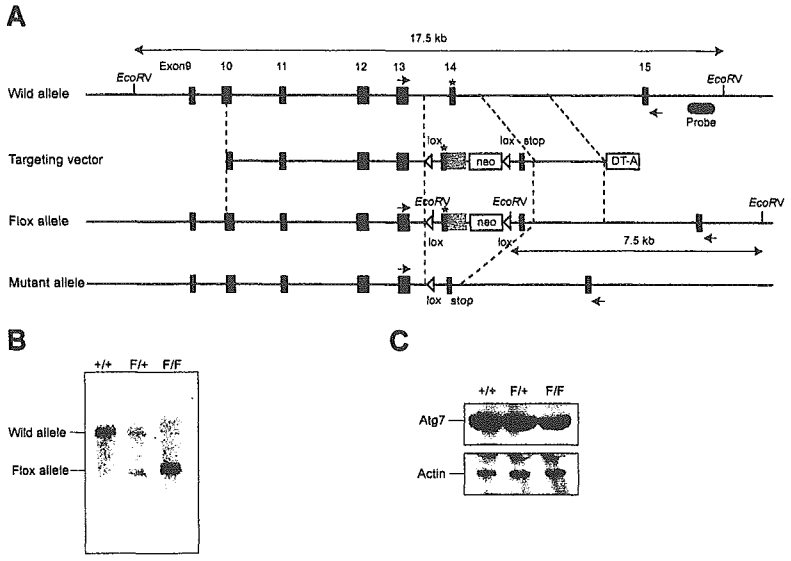

Figure 1. **Generation of *Atg7*$^{F/F}$ mice.** (A) Schematic representation of the targeting vector and the targeted allele of *Atg7* gene. The coding exons numbered in accordance with the initiation site as exon 1 are depicted by black boxes. Green and red boxes indicate *Atg7* cDNA fragment (aa 1786–2097) and *Atg7* cDNA fragment (aa 1669–1698) with stop codon, respectively. The open triangles denote *loxP* sequence. A probe for Southern blot analysis is shown as a gray ellipse. Arrows indicate the positions of PCR primers. The asterisk denotes the essential cysteine residue on exon 14. EcoRV, EcoRV sites; neo, neomycin-resistant gene cassette; DT-A, diphtheria toxin gene. (B) Southern blot analysis of genomic DNAs extracted from mice tails. Wild-type and Flox alleles are detected as 17.5- and 7.5-kb bands, respectively. (C) Immunoblot of Atg7 in MEFs. The lysates of MEFs of indicated genotypes were immunoblotted with Atg7 and actin.

results were also obtained using MEF cells from *Atg7*$^{-/-}$ mice (unpublished data). Together, these results indicate that *Atg7* is crucial for the recycling of amino acids in cells and survival of newborn mice under starvation condition.

Starvation response in adult mice liver

To delete *Atg7* gene in the adult mice, we bred the *Atg7*$^{F/F}$ mice with Mx1-Cre transgenic mice that express the Cre recombinase in response to interferon γ or its chemical inducer, polyinosinic acid–polycytidylic acid (pIpC). The Mx1-Cre transgenic mice can excise Flox allele completely in the liver and spleen and partially in the kidney and heart (Kuhn et al., 1995). Intraperitoneal injections of pIpC resulted in effective recombination of the *Atg7*^{Flox} allele in the liver and spleen (Fig. S2, available at http://www.jcb.org/cgi/content/full/jcb.200412022/DC1; and not depicted). No Atg7 transcript, protein, and activity were detected, similar to *Atg7*$^{-/-}$ mice (Fig. S2). Next, we tested the autophagosome formation under fasting condition. 1-d fasting resulted in induction of typical autophagosomes in control *Atg7*$^{F/+}$:Mx1 mice (Fig. 3, A–D and I). In contrast, no such induction of autophagosome formation was noted in the liver of fasted *Atg7*$^{F/F}$:Mx1 mice (Fig. 3, E, F, and I). Although some autophagosome-like structures were occasionally observed both in fed and fasted mutant mice livers (Fig. 3, G and H), they

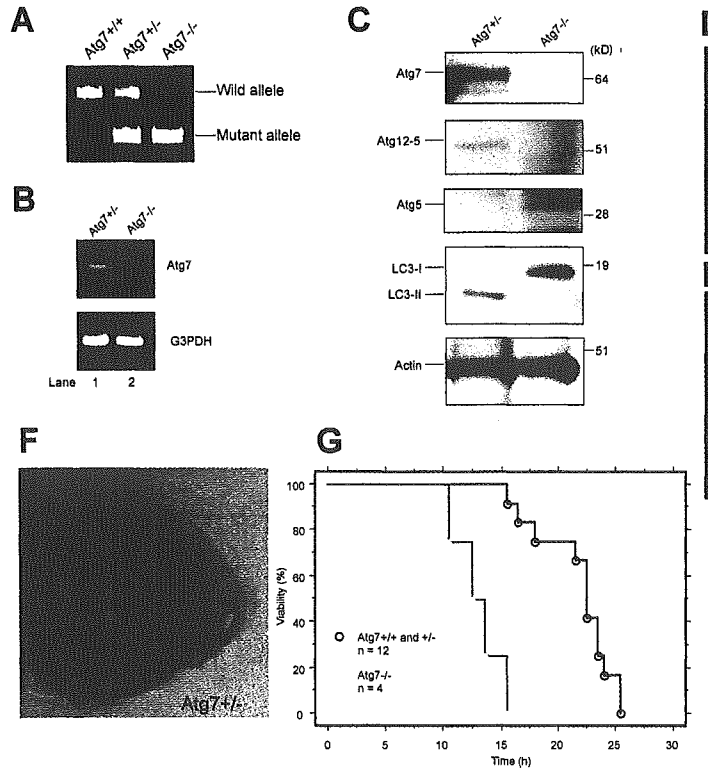

Figure 2. **The phenotypes of *Atg7*-deficient mice.** (A) PCR analysis of genomic DNA extracted from wild-type, *Atg7*$^{+/-}$, and *Atg7*$^{-/-}$ mice tail. The amplified fragments derived from wild and mutant alleles are indicated. (B) Expression of Atg7 transcript. Atg7 transcript was detected by RT-PCR analysis. The region amplified was between exons 12 and 13. G3PDH cDNA was amplified as an internal control. (C) ATG conjugation systems in *Atg7*$^{-/-}$ mice liver. The liver homogenate was centrifuged at 800 *g* for 10 min and the postnuclear supernatant (PNS) was immunoblotted with antibodies against Atg7, Atg5, LC3, and actin as a loading control. The bottom panel of Atg5 blotting is the long exposure of the top panel to detect free Atg5. Data shown are representative of three separate experiments. (D and E) Deficiency of autophagosome formation in *Atg7*$^{-/-}$ heart. *Atg7*$^{+/-}$ (D) and *Atg7*$^{-/-}$ (E) mice expressing GFP-LC3 were obtained by caesarean delivery and analyzed by fluorescence microscopy. Representative results obtained from each neonatal heart at 3 h after caesarean delivery. (F) Morphology of *Atg7*$^{+/-}$ and *Atg7*$^{-/-}$ mice. (G) Kaplan-Meier curves of survival of newborn mice. Control and *Atg7*$^{-/-}$ mice were delivered by caesarean section, and their survival was followed up to 26 h.

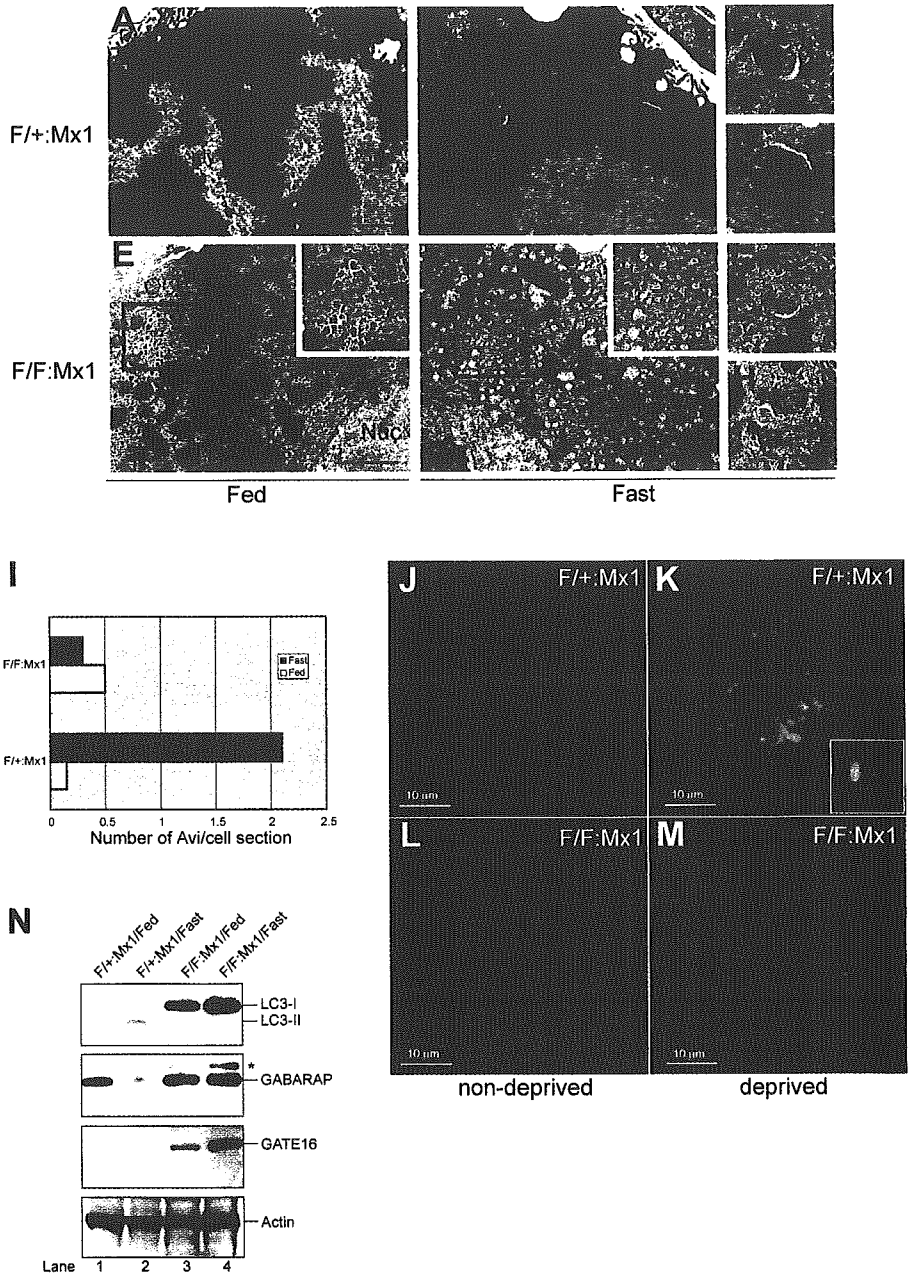

Figure 3. **Impaired autophagosome formation in *Atg7*-deficient liver.** (A–H) Electron micrographs of liver from $Atg7^{F/+}$:Mx1 (A–D) and $Atg7^{F/F}$:Mx1 (E–H) mice fed ad libitum (A and E) or fasted for 1 d (B and F). (C and D) Early stages of autophagic vacuoles observed in B are highlighted. (E and F) Autophagosome was not induced in mutant hepatocytes upon fasting. Insets show higher magnification views of glycogen granules. (G and H) Occasionally observed autophagosome-like structures in mutant hepatocytes. Bars: (A, B, E, and F) 5 μm; (C, D, G, and H) 0.5 μm. (I) Number of autophagosomes per hepatocyte (n = 20) in each genotype was counted and their averages are shown. (J–M) Immunofluorescent analysis of LC3 in primary cultured hepatocytes. Hepatocytes isolated from $Atg7^{F/+}$:Mx1 (J and K) and $Atg7^{F/F}$:Mx1 mice (L and M) were cultured in Williams' E (J and L) or Hanks' solution (K and M). Inset highlights the cup-like structure of LC3 observed in K. (N) Immunoblot analysis of Atg8 homologues in the liver. $Atg7^{F/+}$:Mx1 (lanes 1 and 2) and $Atg7^{F/F}$:Mx1 mice (lanes 3 and 4) were fed ad libitum (lanes 1 and 3) or fasted for 1 d (lanes 2 and 4), and then PNS fractions of liver were analyzed by immunoblotting with anti-LC3, GABARAP, GATE-16, and actin antibodies. Asterisk denotes a nonspecific band. Data shown are representative of three separate experiments.

tended to be smaller than those observed in fasted control liver and hardly contained large cytoplasmic organelles (compare with Fig. 3, C and D). The number of autophagosomes per hepatocyte was counted and the mean values are shown in Fig. 3 I. The mutant hepatocytes lacked typical glycogen area, in contrast to the fed hepatocytes (Fig. 3, A and E); however, well-developed glycogen granules (α granules) were observed between numerous smooth endoplasmic reticula (Fig. 3 E, inset). Immunofluorescent analysis also revealed the presence of many cup-shaped and ringlike structures representing autophagosomes in the control hepatocytes (Fig. 3, J and K). Although several LC3-positive dots were observed in the mutant hepatocytes, they were not induced in response to starvation and did not form cup-shaped and ringlike structures (Fig. 3, L and M).

Next, we examined the fasting response of LC3 and other homologues, GABARAP and GATE-16, by immunoblotting (Fig. 3 N). LC3 is known to be up-regulated and recruited to the autophagosome upon starvation and degraded in the lysosomes (Kabeya et al., 2000). Fasting slightly increased the modification of LC3 in heterozygous liver. In the mutant liver, no modification of LC3 was noted and LC3-I increased in response to fasting. These results suggest that LC3 is up-regulated, but its modification and degradation are impaired in mutant mice. The level of GABARAP did not change upon fasting in the mutant liver, whereas it decreased in the heterozygous liver, suggesting that GABARAP is not up-regulated but its degradation after modification is impaired in mutant liver. Although GATE-16 was hardly detected in the heterozygous liver under both fed and fasting conditions, it was clearly detected

and increased upon fasting in the mutant liver. These results suggest that GATE-16 may be constitutively degraded even at fed condition in heterozygous mice and up-regulated in response to fasting under defective *Atg7*. The levels of all LC3 homologues were elevated even at fed condition in the mutant liver, suggesting their marked stabilization in autophagy-deficient condition. However, the possibility that their transcriptions are up-regulated at basal level due to *Atg7* deficiency cannot be excluded. We sought to determine their localizations in the cells. However, our antibodies for these molecules were not applicable for immunofluorescent analyses, and those localizations remain to be clarified. In conclusion, all Atg8 homologues respond to fasting, although in a different manner, and their levels are affected by the absence of Atg7.

Atg7 is indispensable for fasting-induced degradation of cytosolic proteins and organelles in the mouse liver

Given that autophagosome formation was impaired in *Atg7*-deficient liver, we next examined its effects on the bulk degradation of proteins and organelles under fasting condition. After 1-d fasting in control $Atg7^{F/+}$:Mx1 and mutant $Atg7^{F/F}$:Mx1 mice, the liver was dissected and the amount of total protein per whole liver was measured. The amount of total liver proteins decreased to ~66% by 1-d fasting in the control liver (Fig. 4 A). In contrast, fasting did not significantly decrease the amount of total liver proteins in the mutant liver. Moreover, the amount of total proteins in the mutant liver was 1.5-fold that of control. These results indicate that the decrease of total proteins is dependent on Atg7 and autophagosome formation.

We also examined whether or not fasting causes the degradation of cellular organelles such as mitochondria in the livers of mice. To quantify the amount of the mitochondria, we first measured the activity of mitochondrial enzyme succinate dehydrogenase (SDH) in total liver extracts. In the control livers, fasting was associated with a significant decrease of SDH activity, and the reduction was proportional with the decrease in the amount of total protein (Fig. 4 B). In contrast, fasting was not associated with any change in SDH activity in the mutant livers. Similar to total protein, the basal SDH activity in mutant liver was significantly higher than in control. The effect of fasting on the amount of the mitochondria was also assessed by immunoblot analysis of mitochondrial protein cytochrome *c* (Fig. 4 C). When equal amounts of proteins were loaded, the level of cytochrome *c* was equivalent in the two genotypes at either fed or fasting conditions, suggesting that the ratio of mitochondria versus total protein is not altered by fasting in both genotypes. Considering that the total protein amounts decreased by fasting in the control liver (Fig. 4 A), these results suggest that the mitochondria and cytoplasmic proteins are proportionally degraded upon fasting in heterozygous mice. However, such degradation is impaired in *Atg7*-deficient liver because the levels of both proteins and mitochondria are unchanged and kept at a higher level.

Next, we investigated the effect of autophagy deficiency on protein turnover. To quantify the turnover of long-lived protein, after each control and mutant hepatocytes had been labeled with [^{14}C]leucine for 24 h and chased for 2 h, the release of TCA-soluble [^{14}C]leucine was measured for 4 h. In control hepatocytes, nutrient deprivation significantly induced protein degradation, and such degradation was suppressed by the addition of lysosomal inhibitors such as monomethylamine and E64d and pepstatin (Fig. 4 D). The induced degradation was still observed in the presence of proteasome inhibitor epoxomicin, suggesting that such protein degradation is mediated in the lysosomal pathway rather than the proteasome (Fig. 4 D). In the mutant hepatocytes, degradation of long-lived protein was not induced by nutrient deprivation (Fig. 4 D), indicating that autophagy is the main route for lysosomal degradation under starvation condition. Consistent with these results, amino acid concentrations in starved mutant hepatocytes were lower than in control hepatocytes (unpublished data). Intriguingly, although lysosomal inhibitors inhibited protein degradation even

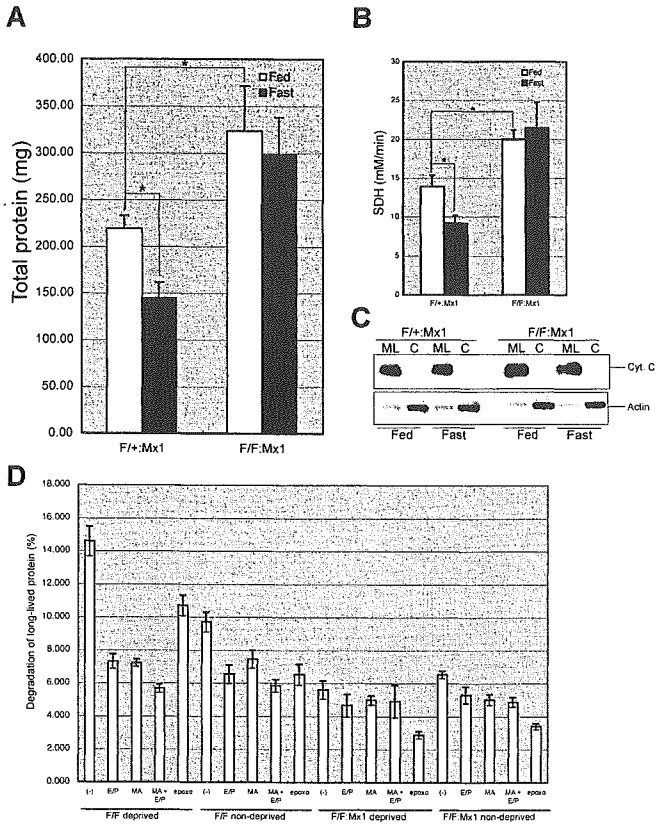

Figure 4. **Fasting response of *Atg7*-deficient liver.** (A and B) Livers from $Atg7^{F/+}$:Mx1 and $Atg7^{F/F}$:Mx1 mice fed ad libitum (Fed) or fasted for 1 d (Fast) at 20 d after pIpC injection were dissected, and the amount of total protein (A) and SDH activity (B) per liver were measured. Data are mean ± SD values of five mice in each group; *, $P < 0.01$. (C) Cytochrome *c* levels in the cytosolic and mitochondria/lysosomal fractions of the liver at 20 d after injection. Equal amount of PNS fractions were centrifuged at 8,000 *g* for 10 min and the pellets were used as the mitochondrial/lysosomal fraction (ML). The supernatants were further centrifuged at 100,000 *g* for 1 h and the supernatant was used as the cytosolic fraction (C). Actin was blotted as control. Data shown are representative of two separate experiments. (D) Turnover of long-lived protein. Hepatocytes from $Atg7^{F/+}$:Mx1 and $Atg7^{F/F}$:Mx1 mice were isolated and labeled with [^{14}C]leucine for 24 h, and degradation of long-lived protein in deprived or nondeprived condition was measured. Monomethylamine (MA) and/or E64d and pepstatin (E/P) or epoxomicin (epoxo) was added as indicated. Data are the mean ± SD of triplicate experiments.

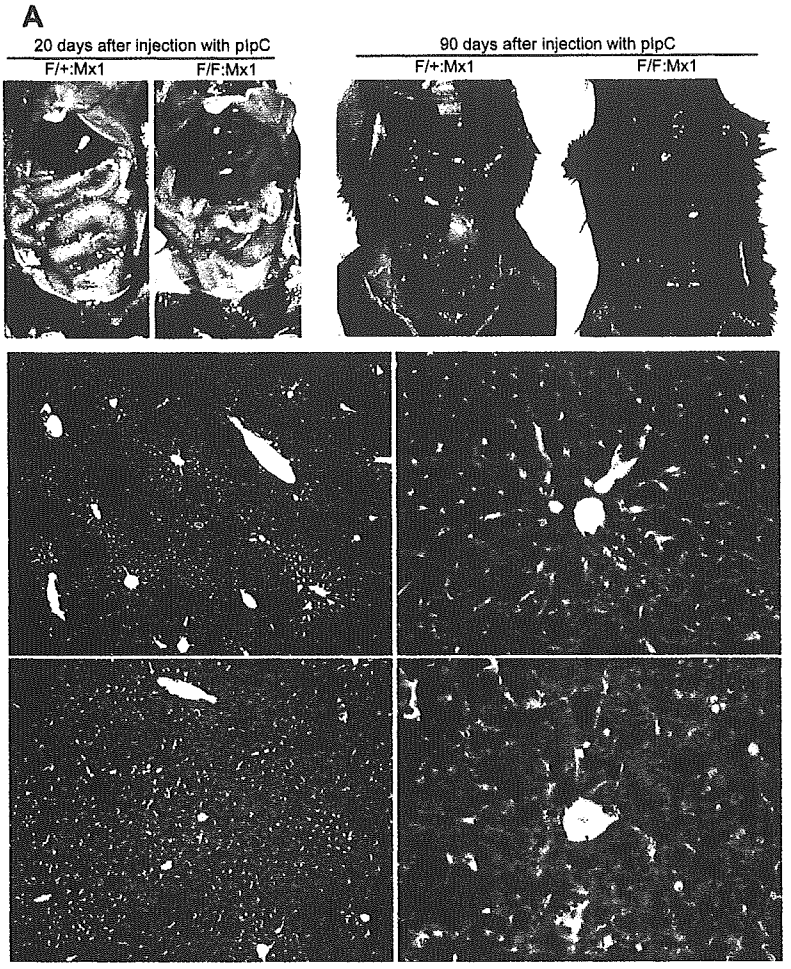

Figure 5. ***Atg7* deficiency in the liver causes hepatomegaly and hepatic cell swelling.** (A) The gross anatomical views of representative mice at the indicated day after pIpC injection. (B–E) Histology of representative livers with *Atg7* deficiency. Hematoxylin and eosin staining of $Atg7^{F/+}$:Mx1 (B and C) and $Atg7^{F/F}$:Mx1 (D and E) liver at 90 d after pIpC injection.

at nondeprived condition in the control hepatocytes, such inhibition was not significant in the mutant hepatocytes (Fig. 4 D), indicating that significant amounts of proteins are constitutively degraded in the lysosome via autophagic pathway. Together, these results suggest that autophagy plays a significant role in turnover of long-lived protein.

Loss of *Atg7* in the liver leads to hepatomegaly and accumulation of abnormal organelles in hepatic cells

We further chased the phenotypes of the mutant mice for up to 90 d after pIpC injection. Gross anatomy revealed severe enlargement of the liver, filling up most of the abdominal cavity (Fig. 5 A). Other major organs were normal histologically (Fig. S3, available at http://www.jcb.org/cgi/content/full/jcb.200412022/DC1). The mean liver weights of control and mutant mice at 90 d after pIpC injection were 1.39 ± 0.24 and 6.10 ± 2.06 g, respectively (n = 5 each). Histological analysis revealed disorganized hepatic lobules and cell swelling in the mutant liver (Fig. 5, D and E). No hepatocellular proliferation or regeneration was detected (unpublished data). Vacuolated hepatic cells were occasionally observed and those were associated with hepatic cell death, which is consistent with the leakage of alkaline phosphatase, aspartate aminotransferase, and alanine aminotransferase in the mutant mice sera (Fig. S4, available at http://www.jcb.org/cgi/content/full/jcb.200412022/DC1).

Although most hepatocytes were still alive in the mutant liver, ultrastructural analysis revealed the appearance of aberrant concentric membranous structures (Fig. 6, A and B), which were also observed as early as 20 d after pIpC-injected liver (not depicted). These structures surrounded various cytoplasmic constituents such as mitochondria, lipid droplets, and vesicular structures (Fig. 6 A). Their membranous elements were continuous with the rough ER (Fig. 6 B, arrowheads), and the corresponding structures were positive for calreticulin, an ER protein marker (not depicted), indicating that these structures originated from the rough ER. Accumulation of peroxisomes (Fig. 6 C) and deformed mitochondria (Fig. 6, C and D) was also observed in the mutant liver. These results suggest the important role of autophagy in turnover of organelles, and its defect results in accumulation of abnormal organelles.

Formation of ubiquitin-positive inclusions in *Atg7*-deficient hepatocytes

Autophagy has been implicated in not only organelle turnover but also in elimination of protein aggregates (Kopito, 2000). Protein aggregates are often ubiquitinated. In the next step, we immunostained the liver with an ubiquitin antibody to examine the presence of such aggregates. Several ubiquitin-positive par-

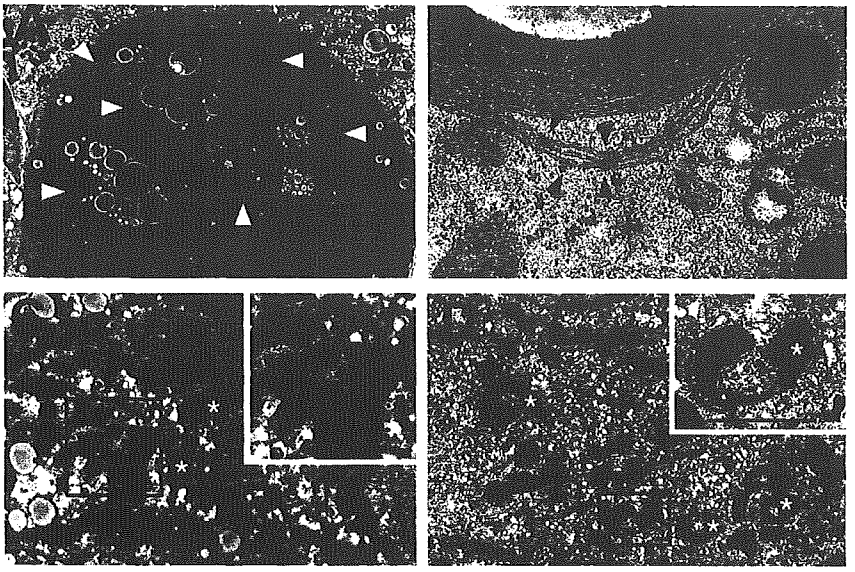

Figure 6. **Electron micrographs of hepatic cells with *Atg7* deficiency.** (A and B) Note the presence of concentric membranous structures in the mutant cells (arrowheads). Higher magnification view (B) shows the membranous elements are continuous with the rough ER (arrowheads). (C and D) The mutant cells contained a high number of peroxisomes (arrows) and deformed mitochondria (asterisks). Insets show higher magnification views. Nuc, nucleus. Bars: (A) 5 μm; (B) 0.5 μm; (C and D) 1 μm.

ticles of various sizes were detected in the $Atg7^{F/F}$:Mx1 but not in $Atg7^{F/+}$:Mx1 hepatic cells at both 10 and 90 d after pIpC injection (Fig. 7, A and B; and Fig. S5, available at http://www.jcb.org/cgi/content/full/jcb.200412022/DC1). The immunoblots of the liver lysates revealed the accumulation of high-molecular mass polyubiquitinated proteins in the mutant liver (Fig. 7 G and Fig. S5), suggesting that the ubiquitin particles are aggregates of polyubiquitinated proteins. To further determine the localization of ubiquitin-positive dots, analysis of immunoelectron micrographs was performed. Numerous particles of colloidal gold, indicative of ubiquitin, were detected on lipid dropletlike structures, membranous structures, and amorphous substances in the cytoplasm (Fig. 7, C–F). Such signals were not observed in the wild-type liver (unpublished data).

The accumulation of ubiquitin-positive inclusions in the cytoplasm prompted us to examine the effect of autophagy deficiency on proteasome function. Immunoblots of proteasome subunits (p112/Rpn2, Mss1/Rpt1, and α5) showed that their relative amounts were not affected in the mutant liver (Fig. 7 G). Furthermore, the activities of the proteasome, measured by Suc-LLVY-MCA as substrate, were also comparable between wild-type and mutant livers (unpublished data). These results indicate the accumulation of ubiquitin-positive aggregates in autophagy-deficient hepatocytes despite the apparently normal proteasome function.

Discussion

Autophagy is a bulk protein degradation pathway, which is conserved in eukaryotes, essential for the survival of unicellular organisms under nutrient-poor condition and for cellular remodeling of multicellular organisms (Mizushima et al., 2002; Levine and Klionsky, 2004). In the present study, we generated conditional knockout mice of *Atg7* gene, which is an essential gene for autophagy in budding yeast, and analyzed its roles in mice.

In mammals, *Atg7* was indeed essential for ATG12 conjugation, LC3 modification systems, and autophagosome formation (Fig. 2, Fig. 3, and Fig. S2). Immunofluorescent analyses revealed that LC3-positive dots appeared but did not form cup-shaped and ringlike structures in $Atg7^{F/F}$:Mx1 livers (Fig. 3). The LC3-I form is usually present at the S100 fraction and the LC3-II form at the P100 fraction (Kabeya et al., 2000). In the mutant liver, LC3-I was present in both S100 and P100 fractions (unpublished data), suggesting that the LC3-positive dots in the mutant hepatocytes are indeed the LC3-I form. These results suggest that LC3 may be recruited to the dot structures independent of the modification (Fig. 3). In mammals, LC3 has at least two homologues, GABARAP and GATE-16, which share common biochemical characteristics (Tanida et al., 2001) and localize to autophagosome in response to fasting (Kabeya et al., 2004). Indeed, the modification and levels of these molecules under fasting condition were affected in the mutant liver (Fig. 3 N). However, these LC3 homologues have been identified in a different biological pathway and may have diverse functions (Ohsumi, 2001). Thus, how their functions and localizations are affected in *Atg7*-deficient cells remains to be clarified.

Although $Atg7^{-/-}$ mice were born at Mendelian ratio, and the major organs were almost normal histologically (Fig. S1), they had reduced body weight and died within 1 d after birth. $Atg7^{-/-}$ mice had lower amino acid level and died earlier compared with wild type under nonsuckling condition after caesarean delivery (Fig. 2 G), suggesting that *Atg7* is important for survival during the early neonatal starvation period, similar to recently reported $Atg5^{-/-}$ mice phenotypes (Kuma et al., 2004). However, because suckling $Atg7^{-/-}$ mice also died within 1 d after birth (unpublished data), the cause of death may not be only due to low level of amino acids. The reason for the reduced body size is also unclear and may be related to placental function or due to inefficient reutilization of nutrients during embryogenesis. It is of note that a lower level of autophagy occurs during embryogenesis (Mizushima et al., 2004) even when nutrients are supplied from the placenta. Furthermore, *Atg7* null mice possess several ubiquitin-positive inclusions in some

organs at the time of birth (unpublished data). This phenotype might be related to the earlier death of mutant. Further analysis of $Atg7^{-/-}$ mice is required to unravel the roles of autophagy, and such analysis is currently under way by breeding the $Atg7^{F/F}$ mice with several Cre-transgenic mice.

Starvation-induced autophagosomes appeared to sequester the cytoplasm randomly (Fig. 3). Consistent with this notion, the amount of mitochondria decreased in proportion with reduction in the amount of total protein (Fig. 4, A–C). These results suggest that mitochondria are degraded nonselectively under fasting condition. In *Atg7*-deficient liver, no autophagosome formation was noted and the degradation of proteins and organelles under fasting condition was largely impaired. These results suggest that the rapid reduction of proteins and organelles upon fasting is dependent on *Atg7* and autophagosome formation.

Although autophagy can be induced by starvation, this pathway may take place even at feeding condition at basal level. This constitutive pathway may be important for turnover of organelles and cytoplasmic proteins. Indeed, the degradation of long-lived protein was inhibited in mutant hepatocytes irrespective of nutrient deprivation (Fig. 4 D), and multiple abnormalities of organelles (e.g., the presence of concentric membranous structure and accumulation of deformed mitochondria) were observed in *Atg7*-deficient hepatocytes (Fig. 6). Unexpectedly, the morphologically abnormal mitochondria appear to retain their function, as judged by the normal membrane potentials and the absence of cytochrome *c* leakage in the cytosol (unpublished data). In contrast to starvation-induced autophagy, whether or not constitutive autophagy eliminates abnormal and excess organelles in a degree of selectivity remains to be clarified.

Beclin 1, a human homologue of *ATG6/VPS30* essential for autophagy in yeast, was recently identified as a tumor suppressor gene, and autophagy has been implicated in the regulation of cellular proliferation (Liang et al., 1999). Indeed, heterozygous disruption of mouse *Beclin 1* led to enhanced tumorigenesis (Qu et al., 2003; Yue et al., 2003). *Atg7* deficiency led to hepatomegaly (Fig. 5 A), suggesting that cell proliferation or malignant transformation might be induced in the *Atg7*-deficient cells. However, neither tumorigenesis nor enhanced cell proliferation was detected as tested by BrdU incorporation at 90 d after pIpC injection in the mutant liver compared with control mice (unpublished data). The hepatomegaly observed in the mutant mice was likely due to increased cellular volume rather than cell number, which is also supported by the swollen appearance of hepatocytes (Fig. 5, D and E).

In *Atg7*-deficient liver, we detected numerous ubiquitin-positive particles indicative of protein aggregates (Fig. 7 and Fig. S5). It has been reported that proteasome inhibition leads to aggregate formation. Conversely, the formation of protein aggregates inhibits the proteasome (Bence et al., 2001), resulting in a malignant cycle of aggregate formation and proteasome inhibition. In the mutant liver, failure of the proteasome was postulated; however, no impairment of proteasome function, in terms of its expression or peptidase activities, was noted (Fig. 7 G and not depicted). Our results suggest that the ubiquitinated proteins eventually aggregate even in the presence of functional proteasomes. Considering that such ubiquitinated aggregates must be difficult to unfold, and proteasomes need to unfold their substrate before degradation (Baumeister et al., 1998), it is likely that elimination of ubiquitin-positive aggregates in the cells is largely dependent on the autophagic process. Protein ubiquitination may also occur after protein aggregation. In either case, we propose the possibility that protein ubiquitination may serve as a signal to the autophagic process in addition to the proteasomes pathway. In this context, it is worth noting that sperm mitochondria are known to be ubiquitinated before degradation during fertilization (Sutovsky et al., 1999). It is now well established that ubiquitin regulates not only proteasomal degradation, but also lysosomal degradation. Thus, it is conceivable that ubiquitin could also regulate the autophagic pathway.

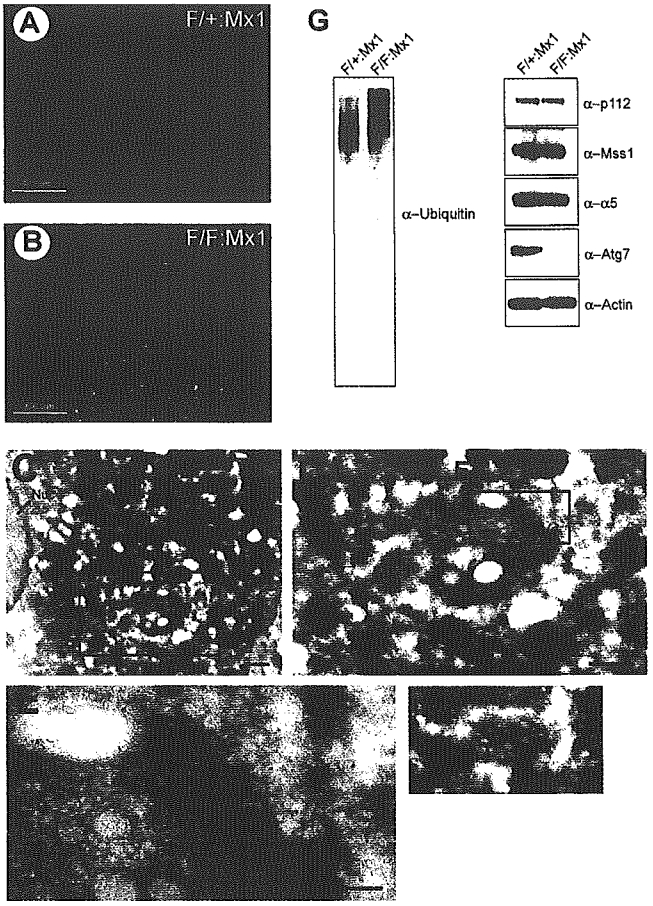

Figure 7. **Accumulation of ubiquitin-positive aggregates in *Atg7*-deficient liver.** (A and B) Immunofluorescent detection of ubiquitin in the $Atg7^{F/+}$:Mx1 (A) and $Atg7^{F/F}$:Mx1 (B) liver. (C–F) Immunoelectron micrographs of ubiquitin in a representative mutant liver. The high-magnification view shows ubiquitin particles near the lipid dropletlike structure (D–F). Bars, 0.5 μm. (G) Immunoblot analysis of the liver. PNS fractions of the liver at 90 d after injection were immunoblotted with the indicated antibodies. Data shown are representative of three separate experiments.

A growing number of disease-associated proteins have been found to accumulate in aggresome, including huntingtin, parkin, α-synuclein, and peripheral myelin protein 22 (Notterpek et al., 1999; Ciechanover and Brundin, 2003). The aggregation of these proteins is thought to be involved in the pathogenesis of Huntington's disease, Parkinson's disease, and peripheral neu-

ropathies, respectively. Enhanced autophagosome formation is prevalent in most of these diseases (Mizushima et al., 2002), and autophagy has also been considered as a caspase-independent cell death pathway (Xue et al., 1999; Bursch, 2001). Our *Atg7* mutant mice should be useful for examining the role of autophagy in the cell death pathway or in a cellular defense mechanism in the pathogenesis of these diseases.

Materials and methods

Generation of *Atg7*$^{f/f}$ mice

The targeting vector was constructed by insertion of a *loxP* sequences within introns 13 and 14 of *Atg7* gene. Exon 14 was fused to a cDNA fragment encoded by exons 15, 16, and 17 (aa 1786–2097) and polyA signal sequence was added after the stop codon. Neo resistant gene cassette (*mc1-neo-pA*) was ligated behind the polyA signal sequence followed by the second *loxP* sequence, splicing acceptor site, and exon 14 with stop codon preceding the active site. We electroporated the targeting vector into mouse TT2 ES cells, selected with 200 μg/ml G418 (GIBCO BRL), and then screened for homologous recombinants by PCR and Southern blot analyses. PCR primers were as follows: 5′-TGGCTGCTACTTCTGCAATGATGT-3′, 5′-GAAGGGACTGGCTGCTATTGGGCGAAGTGC-3′, and 5′-TTAGCACAGGGAACAGCGCTCATGG-3′. Southern blot analysis was performed by digestion of genomic DNA with EcoRV and hybridization with the probe shown in Fig. 1 A. Genotyping of mice by PCR was performed using the following two primers: 5′-TGGCTGCTACTTCTGCAATGATGT-3′ and 5′-CAGGACAGAGACCATCAGCTCCAC-3′. Progeny containing the *Atg7*^{flox} allele were bred with *Zp3*-Cre and *Mx1*-Cre transgenic mice to produce *Atg7*$^{-/-}$ and *Atg7*$^{f/f}$:Mx1 mice, respectively. With regard to *Atg7*$^{f/f}$:Mx1 mice, Cre expression in the liver was induced by i.p. injection of pIpC (Sigma-Aldrich). 300 μl pIpC solution (1 mg/ml in water) was injected three times at 48-h intervals. Mice were housed in specific pathogen-free facilities, and the experimental protocol was approved by the Ethics Review Committee for Animal Experimentation of the Tokyo Metropolitan Institute of Medical Science.

RT-PCR analysis

cDNA was synthesized from 5 μg of DNase I–treated total RNA using the SuperScript First-Strand Synthesis System (GIBCO BRL) and oligo $(dT)_{12\text{-}18}$ primers. Specific primers for each gene were as follows: 5′-ATGCCAGGACACCCTGTGAACTTC-3′ and 5′-ACATCATTGCAGAAGTAGCAGCCA-3′ for Atg7, and 5′-GAGCTGAACGGGAAGCTCAC-3′ and 5′-ACCACCCTGTTGCTGTAGC-3′ for G3PDH.

Immunoblot analysis

The fractions were immunoblotted as described previously (Komatsu et al., 2001). The antibodies for Atg7 (Tanida et al., 1999) and Atg5 (Mizushima et al., 2001) were described previously. The antibodies for ubiquitin (DakoCytomation) and actin (MAB1501R; Chemicon International, Inc.) were purchased. The antibodies against LC3, GABARAP, and GATE-16 were raised in rabbits using their specific peptides as antigens. The antibodies against p112, Mss1, and α5 were provided by K.B. Hendil (August Krogh Institute, University of Copenhagen, Copenhagen, Denmark).

Caesarean delivery and measurement of amino acids

Newborns were delivered by caesarean section at 19.0 d postcoitus and placed in a humidified, thermostat-controlled chamber (30°C). Plasma was fixed in 3% sulphosalicylic acid. Amino acids in the supernatant from plasma samples were measured by an amino acid analyzer (L8500A; Hitachi).

Protein degradation assay

The assay was performed essentially as described previously (Gronostajski and Pardee, 1984). In brief, hepatocytes were plated at 5×10^4 cells/well in collagen-coated 24-well plates and cultured in Williams' E medium with 10% FCS (Williams' E/10% FCS) for 24 h. Cells were incubated with Williams' E/10% FCS containing 0.5 μCi/ml [^{14}C]leucine for 24 h to label long-lived proteins. Cells were washed with Williams' E/10% FCS containing 2 mM of unlabeled leucine and incubated with the medium for 2 h to allow degradation of short-lived proteins and minimize the incorporation of labeled leucine, which was released by proteolysis into protein. The cells were then washed with PBS and incubated at 37°C with Krebs-Ringer bicarbonate medium and Williams' E/10% FCS in the presence or absence of protease inhibitors (5 mM monomethylamine, 10 μg/ml E64d and pepstatin, or 5 μM epoxomicin). After 4 h, aliquots of the medium were taken and a one-tenth volume of 100% trichloroacetic acid was added to each aliquot. The mixtures were centrifuged at 12,000 *g* for 5 min, and the acid-soluble radioactivity was determined using a liquid scintillation counter. At the end of the experiment, the cultures were washed twice with PBS, and 1 ml of cold trichloroacetic acid was added to fix the cell proteins. The fixed cell monolayers were washed with trichloroacetic acid and dissolved in 1 ml of 1 N NaOH at 37°C. Radioactivity in an aliquot of 1 N NaOH was determined by liquid scintillation counting. The percentage of protein degradation was calculated according to published procedures (Gronostajski and Pardee, 1984).

Histological examination

Tissues were dissected, fixed in 4% PFA, paraffin embedded, and sectioned. Sections were stained by Meyer's hematoxylin and eosin. For immunohistochemical analysis, sections were blocked in 5% normal goat serum in PBS containing 0.2% Triton X-100, and then incubated with antiubiquitin antibody (1B3; MBL International Corporation) and Alexa 488–labeled secondary antibody (Molecular Probes). Apoptotic cells were detected by TUNEL assay using Apoptag kit (Intergen Company) as described previously (Tateishi et al., 2001). For GFP-LC3 observations, tissues were fixed with 4% PFA, and the cryosections were imaged with a conventional fluorescence microscope. For LC3 staining, hepatocytes were fixed and stained with anti-LC3 antibody as described previously (Kabeya et al., 2000). All fluorescence images were obtained using a fluorescence microscope (model Q550FV; Leica) equipped with cooled charge-coupled device camera (model CTR MIC; Leica). Pictures were taken using Qfluoro software (Leica).

EM and immunoelectron microscopy

Livers were fixed by cardiac perfusion using 0.1 M phosphate buffer containing 2% PFA and 2% glutaraldehyde for conventional EM. They were post-fixed with 1% OsO_4, embedded in Epon812, and sectioned. Immunoelectron microscopy was performed on cryothin sections as described previously (Waguri et al., 1995). In brief, livers were frozen in phosphate buffer with 2.3 M sucrose and 20% polyvinyl pyrrhoridon. Ultrathin sections were mounted on Formvar carbon-coated nickel grids, blocked with 1% BSA in PBS, and incubated with antiubiquitin antibody (1B3) and colloidal gold conjugated secondary antibody.

Other procedures

MEFs were prepared as described previously (Murata et al., 2001). Primary hepatocytes were prepared as described previously (Ueno et al., 1990). Cell starvation was conducted by incubating the cells in Hanks' balanced solution after three separate washes. The SDH activity was assayed as described previously (Ueno et al., 1990).

On line supplemental material

Fig. S1 shows the histological analyses of tissues from *Atg7*$^{+/-}$ and *Atg7*$^{-/-}$ mice at 1 d after birth. Fig. S2 shows the loss of Atg7 protein and activity in *Atg7*$^{f/f}$:Mx1 mouse liver. Fig. S3 shows the histological analyses of tissues from *Atg7*$^{f/+}$:Mx1 and *Atg7*$^{f/f}$:Mx1 mice. Fig. S4 shows the cell death in autophagy-deficient liver. Fig. S5 shows the accumulation of ubiquitin-positive inclusions at early stage of autophagy deficiency. Further comments on the data can be found in the legends. Online supplemental material is available at http://www.jcb.org/cgi/content/full/jcb.200412022/DC1.

We thank T. Kaneko, T. Kouno, and K. Tatsumi for technical assistance. We also thank F. Kaji for his help in EM study; A. Kuma for technical guidance in caesarean delivery; K. Tateishi and H. Uozaki for discussion of liver pathology; and T. Fujimura and K. Murayama for amino acid measurements.

This work was supported in part by Grants-in-Aid from the Ministry of Education, Culture, Sports, Science and Technology of Japan.

Submitted: 3 December 2004
Accepted: 22 March 2005

References

Baumeister, W., J. Walz, F. Zuhl, and E. Seemuller. 1998. The proteasome: paradigm of a self-compartmentalizing protease. *Cell.* 92:367–380.

Bence, N.F., R.M. Sampat, and R.R. Kopito. 2001. Impairment of the ubiquitin-proteasome system by protein aggregation. *Science.* 292:1552–1555.

Bursch, W. 2001. The autophagosomal-lysosomal compartment in programmed cell death. *Cell Death Differ.* 8:569–581.

Ciechanover, A., and P. Brundin. 2003. The ubiquitin proteasome system in neurodegenerative diseases: sometimes the chicken, sometimes the egg. *Neuron.* 40:427–446.

Dunn, W.A., Jr. 1994. Autophagy and related mechanisms of lysosome-mediated protein degradation. *Trends Cell Biol.* 4:139–143.

Goldberg, A.L. 2003. Protein degradation and protection against misfolded or damaged proteins. *Nature.* 426:895–899.

Gronostajski, R.M., and A.B. Pardee. 1984. Protein degradation in 3T3 cells and tumorigenic transformed 3T3 cells. *J. Cell. Physiol.* 119:127–132.

Hanaoka, H., T. Noda, Y. Shirano, T. Kato, H. Hayashi, D. Shibata, S. Tabata, and Y. Ohsumi. 2002. Leaf senescence and starvation-induced chlorosis are accelerated by the disruption of an *Arabidopsis* autophagy gene. *Plant Physiol.* 129:1181–1193.

Ichimura, Y., T. Kirisako, T. Takao, Y. Satomi, Y. Shimonishi, N. Ishihara, N. Mizushima, I. Tanida, E. Kominami, M. Ohsumi, et al. 2000. A ubiquitin-like system mediates protein lipidation. *Nature.* 408:488–492.

Kabeya, Y., N. Mizushima, T. Ueno, A. Yamamoto, T. Kirisako, T. Noda, E. Kominami, Y. Ohsumi, and T. Yoshimori. 2000. LC3, a mammalian homologue of yeast Apg8p, is localized in autophagosome membranes after processing. *EMBO J.* 19:5720–5728.

Kabeya, Y., N. Mizushima, A. Yamamoto, S. Oshitani-Okamoto, Y. Ohsumi, and T. Yoshimori. 2004. LC3, GABARAP and GATE16 localize to autophagosomal membrane depending on form-II formation. *J. Cell Sci.* 117:2805–2812.

Klionsky, D.J., and S.D. Emr. 2000. Autophagy as a regulated pathway of cellular degradation. *Science.* 290:1717–1721.

Komatsu, M., I. Tanida, T. Ueno, M. Ohsumi, Y. Ohsumi, and E. Kominami. 2001. The C-terminal region of an Apg7p/Cvt2p is required for homodimerization and is essential for its E1 activity and E1-E2 complex formation. *J. Biol. Chem.* 276:9846–9854.

Kopito, R.R. 2000. Aggresomes, inclusion bodies and protein aggregation. *Trends Cell Biol.* 10:524–530.

Kuhn, R., F. Schwenk, M. Aguet, and K. Rajewsky. 1995. Inducible gene targeting in mice. *Science.* 269:1427–1429.

Kuma, A., M. Hatano, M. Matsui, A. Yamamoto, H. Nakaya, T. Yoshimori, Y. Ohsumi, T. Tokuhisa, and N. Mizushima. 2004. The role of autophagy during the early neonatal starvation period. *Nature.* 432:1032–1036.

Levine, B., and D.J. Klionsky. 2004. Development by self-digestion: molecular mechanisms and biological functions of autophagy. *Dev. Cell.* 6:463–477.

Lewandoski, M., K.M. Wassarman, and G.R. Martin. 1997. Zp3-cre, a transgenic mouse line for the activation or inactivation of loxP-flanked target genes specifically in the female germ line. *Curr. Biol.* 7:148–151.

Liang, X.H., S. Jackson, M. Seaman, K. Brown, B. Kempkes, H. Hibshoosh, and B. Levine. 1999. Induction of autophagy and inhibition of tumorigenesis by beclin 1. *Nature.* 402:672–676.

Massey, A., R. Kiffin, and A.M. Cuervo. 2004. Pathophysiology of chaperone-mediated autophagy. *Int. J. Biochem. Cell Biol.* 36:2420–2434.

Mizushima, N., T. Noda, T. Yoshimori, Y. Tanaka, T. Ishii, M.D. George, D.J. Klionsky, M. Ohsumi, and Y. Ohsumi. 1998. A protein conjugation system essential for autophagy. *Nature.* 395:395–398.

Mizushima, N., A. Yamamoto, M. Hatano, Y. Kobayashi, Y. Kabeya, K. Suzuki, T. Tokuhisa, Y. Ohsumi, and T. Yoshimori. 2001. Dissection of autophagosome formation using Apg5-deficient mouse embryonic stem cells. *J. Cell Biol.* 152:657–668.

Mizushima, N., Y. Ohsumi, and T. Yoshimori. 2002. Autophagosome formation in mammalian cells. *Cell Struct. Funct.* 27:421–429.

Mizushima, N., A. Yamamoto, M. Matsui, T. Yoshimori, and Y. Ohsumi. 2004. In vivo analysis of autophagy in response to nutrient starvation using transgenic mice expressing a fluorescent autophagosome marker. *Mol. Biol. Cell.* 15:1101–1111.

Mortimore, G.E., and A.R. Poso. 1987. Intracellular protein catabolism and its control during nutrient deprivation and supply. *Annu. Rev. Nutr.* 7:539–564.

Murata, S., H. Udono, N. Tanahashi, N. Hamada, K. Watanabe, K. Adachi, T. Yamano, K. Yui, N. Kobayashi, M. Kasahara, et al. 2001. Immunoproteasome assembly and antigen presentation in mice lacking both PA28alpha and PA28beta. *EMBO J.* 20:5898–5907.

Nakagawa, I., A. Amano, N. Mizushima, A. Yamamoto, H. Yamaguchi, T. Kamimoto, A. Nara, J. Funao, M. Nakata, K. Tsuda, et al. 2004. Autophagy defends cells against invading group *A Streptococcus*. *Science.* 306:1037–1040.

Nishino, I., J. Fu, K. Tanji, T. Yamada, S. Shimojo, T. Koori, M. Mora, J.E. Riggs, S.J. Oh, Y. Koga, et al. 2000. Primary LAMP-2 deficiency causes X-linked vacuolar cardiomyopathy and myopathy (Danon disease). *Nature.* 406:906–910.

Notterpek, L., M.C. Ryan, A.R. Tobler, and E.M. Shooter. 1999. PMP22 accumulation in aggresomes: implications for CMT1A pathology. *Neurobiol. Dis.* 6:450–460.

Ohsumi, Y. 2001. Molecular dissection of autophagy: two ubiquitin-like systems. *Nat. Rev. Mol. Cell Biol.* 2:211–216.

Perlmutter, D.H. 2002. Liver injury in alpha1-antitrypsin deficiency: an aggregated protein induces mitochondrial injury. *J. Clin. Invest.* 110:1579–1583.

Qu, X., J. Yu, G. Bhagat, N. Furuya, H. Hibshoosh, A. Troxel, J. Rosen, E.L. Eskelinen, N. Mizushima, Y. Ohsumi, et al. 2003. Promotion of tumorigenesis by heterozygous disruption of the beclin 1 autophagy gene. *J. Clin. Invest.* 112:1809–1820.

Seglen, P.O., and P. Bohley. 1992. Autophagy and other vacuolar protein degradation mechanisms. *Experientia.* 48:158–172.

Shintani, T., and D.J. Klionsky. 2004. Autophagy in health and disease: a double-edged sword. *Science.* 306:990–995.

Shintani, T., N. Mizushima, Y. Ogawa, A. Matsuura, T. Noda, and Y. Ohsumi. 1999. Apg10p, a novel protein-conjugating enzyme essential for autophagy in yeast. *EMBO J.* 18:5234–5241.

Sutovsky, P., R.D. Moreno, J. Ramalho-Santos, T. Dominko, C. Simerly, and G. Schatten. 1999. Ubiquitin tag for sperm mitochondria. *Nature.* 402:371–372.

Tanaka, Y., G. Guhde, A. Suter, E.L. Eskelinen, D. Hartmann, R. Lullmann-Rauch, P.M. Janssen, J. Blanz, K. von Figura, and P. Saftig. 2000. Accumulation of autophagic vacuoles and cardiomyopathy in LAMP-2-deficient mice. *Nature.* 406:902–906.

Tanida, I., N. Mizushima, M. Kiyooka, M. Ohsumi, T. Ueno, Y. Ohsumi, and E. Kominami. 1999. Apg7p/Cvt2p: a novel protein-activating enzyme essential for autophagy. *Mol. Biol. Cell.* 10:1367–1379.

Tanida, I., E. Tanida-Miyake, T. Ueno, and E. Kominami. 2001. The human homolog of *Saccharomyces cerevisiae* Apg7p is a protein-activating enzyme for multiple substrates including human Apg12p, GATE-16, GABARAP, and MAP-LC3. *J. Biol. Chem.* 276:1701–1706.

Tateishi, K., M. Omata, K. Tanaka, and T. Chiba. 2001. The NEDD8 system is essential for cell cycle progression and morphogenetic pathway in mice. *J. Cell Biol.* 155:571–579.

Tsukada, M., and Y. Ohsumi. 1993. Isolation and characterization of autophagy-defective mutants of *Saccharomyces cerevisiae*. *FEBS Lett.* 333:169–174.

Ueno, T., S. Watanabe, M. Hirose, T. Namihisa, and E. Kominami. 1990. Phalloidin-induced accumulation of myosin in rat hepatocytes is caused by suppression of autolysosome formation. *Eur. J. Biochem.* 190:63–69.

Waguri, S., N. Sato, T. Watanabe, K. Ishidoh, E. Kominami, K. Sato, and Y. Uchiyama. 1995. Cysteine proteinases in GH4C1 cells, a rat pituitary tumor cell line, are secreted by the constitutive and regulated secretory pathways. *Eur. J. Cell Biol.* 67:308–318.

Xue, L., G.C. Fletcher, and A.M. Tolkovsky. 1999. Autophagy is activated by apoptotic signalling in sympathetic neurons: an alternative mechanism of death execution. *Mol. Cell. Neurosci.* 14:180–198.

Yue, Z., S. Jin, C. Yang, A.J. Levine, and N. Heintz. 2003. Beclin 1, an autophagy gene essential for early embryonic development, is a haploinsufficient tumor suppressor. *Proc. Natl. Acad. Sci. USA.* 100:15077–15082.